

# NH<sub>3</sub>-promoted hydrolysis of NO<sub>2</sub> induces explosive growth in HONO

Wanyun Xu<sup>1</sup>, Ye Kuang<sup>2,\*</sup>, Chunsheng Zhao<sup>3</sup>, Jiangchuan Tao<sup>2</sup>, Gang Zhao<sup>3</sup>, Yuxuan Bian<sup>4</sup>,  
Wen Yang<sup>5</sup>, Yingli Yu<sup>3</sup>, Chuanyang Shen<sup>3</sup>, Linlin Liang<sup>1</sup>, Gen Zhang<sup>1</sup>, Weili Lin<sup>6</sup>,  
Xiaobin Xu<sup>1</sup>

<sup>1</sup> State Key Laboratory of Severe Weather, Key Laboratory for Atmospheric Chemistry, Institute of Atmospheric Composition, Chinese Academy of Meteorological Sciences, Beijing, 100081, China.

<sup>2</sup> Institute for Environmental and Climate Research, Jinan University, Guangzhou, China.

<sup>3</sup> Department of Atmospheric and Oceanic Sciences, School of Physics, Peking University, Beijing, China

<sup>4</sup> State Key Laboratory of Severe Weather, Chinese Academy of Meteorological Sciences, Beijing, 100081, China

<sup>5</sup> State Key Laboratory of Environmental Criteria and Risk Assessment, Chinese Research Academy of Environmental Sciences, Beijing, 100081, China

<sup>6</sup> College of Life and Environmental Sciences, Minzu University of China, Beijing, 100081, China

Corresponding author: Ye Kuang (kuangye@jnu.edu.cn)

## Abstract

The study of atmospheric nitrous acid (HONO), which is the primary source of OH radicals, is crucial to atmospheric photochemistry and heterogeneous chemical processes. The heterogeneous NO<sub>2</sub> chemistry under haze conditions was pointed out to be one of the missing sources of HONO on the North China Plain, producing sulfate and nitrate in the process. However, controversy exists between various proposed mechanisms, mainly debating on whether SO<sub>2</sub> directly takes part in the HONO production process and what roles NH<sub>3</sub> and the pH value play in it. In this paper, never before seen explosive HONO production (maximum rate: 16 ppb/hour) was reported and evidence was found for the first time in field measurements during fog episodes (usually with 4<pH<5<6) and haze episodes under high relative humidity (usually with pH<5<4), that NH<sub>3</sub> was the key factor that promoted the hydrolysis of NO<sub>2</sub>, leading to explosive growth of HONO and nitrate under both high and lower pH conditions. The results also suggest that SO<sub>2</sub> does not directly take part in the HONO formation during fog and haze events, but was indirectly oxidized upon the photolysis of HONO through subsequent radical mechanisms. Aerosol hygroscopicity significantly increased with the rapid inorganic secondary aerosol formation further promoting the HONO production- as a positive feedback. For future

带格式的: 两端对齐

设置了格式: 字体: 宋体

photochemical and aerosol pollution abatement, it is crucial to introduce effective  $\text{NH}_3$  emission control measures, since the  $\text{NH}_3$ -promoted  $\text{NO}_2$  hydrolysis is a large daytime HONO source, releasing large amounts of OH radicals upon photolysis, which will contribute largely to both atmospheric photochemistry and secondary aerosol formation.

## 1 Introduction

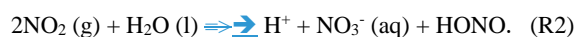
Nitrous acid (HONO) plays a vital role in atmospheric chemistry due to the fact that its photolysis is a major source (Michoud et al., 2014; Kleffmann et al., 2005) of hydroxyl radical (OH) which determines the atmospheric oxidative capacity and plays crucial role in tropospheric chemistry in processes such as the ozone formation, the degradation of volatile organic compounds and the secondary aerosol formation (Cheng et al., 2016; Wang et al., 2016). Hence, the source study of nitrous acid (HONO) is of crucial importance for the understanding of the tropospheric chemistry, for chemistry and climate modelling and for developing effective pollution control strategies (Lu et al., 2018).

The North China Plain (NCP) is troubled by the persistent complex air pollution with high loadings of both photochemical pollutants and particulate pollution (Zheng et al., 2015; Ran et al., 2011) and the simultaneous mitigation of the two types of pollution has encountered trouble due to the nonlinear dependence of ozone on  $\text{NO}_x$  (Xing et al., 2018). Unknown daytime sources of HONO caught attention during the past few years (Michoud et al., 2014; Liu et al., 2014; Su et al., 2011) and results from a recent study indicate that an additional missing source is required to explain more than 50% of observed HONO concentration in the daytime in Western China. Results from several recent studies demonstrate that intense heterogeneous conversion of  $\text{NO}_2$  to HONO on particle surfaces might be a significant source of HONO (Liu et al., 2014; Cui et al., 2018).

Two main HONO heterogeneous production pathways involving aerosol water and  $\text{NO}_2$  were proposed. In light of drastic decrease of solar radiation during severe haze events and rich ammonia conditions on the NCP, the first pathway hypothesized that  $\text{NO}_2$  (g) dissolved in aerosol water at aerosol  $\text{pH} > 5.5$  rapidly formed HONO while oxidizing  $\text{HSO}_3^-$  (aq) to sulfate. The stoichiometry of this mechanism is as follows (Cheng et al., 2016; Wang et al., 2016):



Based on this mechanism, good agreement between modelled and observed sulfate formation rates were achieved. However, the assumption that the pH of ambient aerosols can reach beyond 5.5 is a debatable issue. Results from several most recent studies indicate that the pH of ambient aerosols fall in the range of 3-5 in most cases (Ding et al., 2018; Liu et al., 2017a; Song et al., 2018). Given this, it was proposed that HONO and  $\text{NO}_2^-$  were produced in the hydrolysis process of  $\text{NO}_2$ , releasing OH radicals upon photolysis, which indirectly oxidize  $\text{SO}_2$  to sulfate (Li et al., 2018b) (Li et al., 2018b):



Results of Yabushita et al. (2009) suggest that anions (such as  $\text{Cl}^-$ ,  $\text{Br}^-$  and  $\text{I}^-$ ) greatly enhance the hydrolysis of  $\text{NO}_2$  on water, and the  $\text{NO}_2$  uptake coefficients of R2 can be enhanced several orders of magnitude by increasing electrolyte concentration. The ambient aerosol particles in the boundary layer are in aqueous phase under high RH (Liu et al., 2017b) and the aerosol or fog water is not pure with different dissolved anions (Wu et al., 2018; Lu et al., 2010). Therefore, HONO and nitrate formed through this mechanism should be independent of aerosol acidity, and should be primarily affected by the aerosol surface area density, aerosol liquid water content and  $\text{NO}_2$  concentration (Li et al., 2018b) (Li et al., 2018b). Moreover, recent theoretical simulations have proposed a HONO formation mechanism involving  $\text{NO}_2$  and water and have identified that  $\text{NH}_3$  can promote the hydrolysis of  $\text{NO}_2$  (Li et al., 2018a) (R2). Despite of this, no direct evidence from field observations were available in this paper to support their findings.

Although the proposed HONO formation mechanisms are all heterogeneous reactions of  $\text{NO}_2$ , the details of how  $\text{SO}_2$ , pH and  $\text{NH}_3$  are involved in heterogeneous formation are still under debate (Li et al., 2018b) (Li et al., 2018b) and a clear mechanism is still missing in current models to explain both the daytime concentration of observed HONO and the secondary inorganic aerosol formation. Measurements of HONO are rare and simultaneous observations of HONO and aerosol physical and chemical characteristics are lacking to thoroughly analyze or directly support the aerosol heterogeneous HONO formation mechanisms involving  $\text{NO}_2$ . In this paper, we present for the first time simultaneous measurements of HONO, sulfate and nitrate as well as other precursor gases, oxidants and meteorological parameters during both fog and haze episodes under high

ambient RH. Fog water pH is usually greater than 5.5 in eastern China (Safai et al., 2008; Lu et al., 2010), while calculations in this work and previous studies collectively indicate a moderately acidic condition ( $4 < \text{pH} < 5$ ) for fine particles in northern China winter haze. The observational results unveil that  $\text{NH}_3$  is the key factor that promotes the hydrolysis of  $\text{NO}_2$ , resulting in explosive formation of HONO, nitrate and sulfate.

## 2 Site description and instruments

From 15<sup>th</sup> Oct. to 25<sup>th</sup> Nov. 2016, a field campaign intended to study sulfate formation was conducted at the Ecological and Agricultural Meteorology Station ( $39^\circ 09' \text{N}$ ,  $115^\circ 44' \text{E}$ ) of the Chinese Academy of Meteorological Sciences. The site is partly composed of experimental farmland and is also surrounded by farmland and small residential towns (nearest town  $\sim 1.5$  km). It is located between Beijing ( $\sim 100$  km) and Baoding ( $\sim 40$  km), two megacities on the North China Plain (Fig. 1). During this field campaign, an In situ Gas and Aerosol Compositions Monitor (IGAC, Fortelice International Co., Taiwan) was used for monitoring water-soluble ions ( $\text{Na}^+$ ,  $\text{K}^+$ ,  $\text{Ca}^{2+}$ ,  $\text{Mg}^{2+}$ ,  $\text{NH}_4^+$ ,  $\text{SO}_4^{2-}$ ,  $\text{NO}_3^-$ ,  $\text{NO}_2^-$ ,  $\text{Cl}^-$ ) of  $\text{PM}_{2.5}$  (particulate matter with aerodynamic diameter less than  $2.5 \mu\text{m}$ ) and trace gases including HONO,  $\text{SO}_2$ ,  $\text{NH}_3$ , HCl, and  $\text{HNO}_3$  with a time resolution of 1 h. The IGAC system draws in ambient air through a  $\text{PM}_{10}$  inlet and passes the sample through a sharp-cut  $\text{PM}_{2.5}$  cyclone at a flowrate of  $16.7 \text{ L} \cdot \text{min}^{-1}$ . The total length of the stainless steel sampling line is approximately 2 m, with an inner diameter of 3.18 cm (1.25 inch), resulting in a residence time below 6 s, suggesting that underestimates in  $\text{NH}_3$  possibly caused by adsorption on the stainless steel sampling tube as was proposed by Young et al. (2016) might be unimportant. A vertical annular denuder wetted with dilute  $\text{H}_2\text{O}_2$  solution ( $5 \times 10^{-3} \text{ M}$ ) collects the trace gases and converts  $\text{SO}_2$  rapidly to  $\text{SO}_4^{2-}$ , preventing  $\text{SO}_2$  from reacting with  $\text{NO}_2$  in the absorption solution to produce HONO artefacts. A scrub and impact aerosol collector under the denuder is mounted at an inclined angle to capture particles based on impaction after condensation growth. Two separate Ion Chromatographs are used to respectively analyze anions and cations for the gas and aerosol liquid extracts which were injected from the denuder and the aerosol collector once an hour. The detection limits are below  $0.12 \mu\text{g} \cdot \text{m}^{-3}$  and the background concentration of most water-soluble inorganic ions within the instrument were below  $0.11 \mu\text{g} \cdot \text{m}^{-3}$ , only with  $\text{SO}_4^{2-}$  showing a background concentration of  $1.10 \mu\text{g} \cdot \text{m}^{-3}$  (Young et al., 2016). Under highly polluted conditions such as our site  $\text{m}^{-3}$  (Young et al., 2016). Considering the severe pollution state

the NCP is under, these measurement uncertainties are fully acceptable. The instrument has shown good performance in the past, agreeing well with filter based samples (Liu et al., 2017a)(Liu et al., 2017a). Standard LiBr solution was continuously added to the aerosol liquid extracts during the measurements, to ensure the sampling and analyzing process is stable. The swing amplitude was within the range of three standard deviation, confirming the stability of the ion analyzing system throughout the campaign. A mixed standard solution was diluted to perform multipoint calibrations (at 5, 10, 20, 50, 100, 200, 500 and 1000 ppb concentrations) at the beginning and at the end of the campaign for the ions  $\text{Na}^+$ ,  $\text{K}^+$ ,  $\text{Ca}^{2+}$ ,  $\text{Mg}^{2+}$ ,  $\text{NH}_4^+$ ,  $\text{Li}^+$ ,  $\text{SO}_4^{2-}$ ,  $\text{NO}_3^-$ ,  $\text{NO}_2^-$ ,  $\text{Cl}^-$ ,  $\text{Br}^-$ , with the  $R^2$  of the calibrations reaching above 0.9999. A comparison between  $\text{NH}_3$  observed by IGAC and by an economical  $\text{NH}_3$  analyser (LGR, DLT-100, details see Meng et al. (2018)) yielded an overall slope of 0.91 with  $R=0.63$  (Fig.S1a). A better comparison result (slope of 1.03,  $R=0.74$ ) would be obtained if data associated with  $\text{RH}>80$  were excluded (Fig.S1b). The overestimation of LGR instruments compared to denuder based instruments has also been reported in Teng et al. (2017), suggesting possible interference of water vapor on  $\text{NH}_3$  measurements. As can be seen in Fig.S2, both instruments captured the same the diurnal variation of  $\text{NH}_3$  during the four case episodes in this study, which proves that the IGAC instrument was able to capture the overall variation trends of  $\text{NH}_3$ . Since both instruments have their uncertainties, we decided to use the  $\text{NH}_3$  measured by the IGAC instrument for better consistency with the other data.

$\text{NO}_x$  and CO were observed using commercial instruments from Thermo Electronics (Model 42CTL and 48CTL), while the Aerolaser AL2021  $\text{H}_2\text{O}_2$ -monitor was used to measure  $\text{H}_2\text{O}_2$  concentrations. The ambient RH, temperature, wind speed and wind direction were observed using an automatic weather station. The dry state particle number size distributions (PNSDs) in the diameter range of 3nm to 10 $\mu\text{m}$ , were jointly measured by a scanning mobility particle size spectrometer (SMPS) and an Aerodynamic Particle Sizer (APS, TSI Inc., Model 3321). The ambient aerosol liquid water concentrations were calculated based on measurements of a three-wavelengthwavelength humidified nephelometer system (Kuang et al., 2018). The aerosol hygroscopicity parameter  $\kappa$  (Petters and Kreidenweis, 2007) is calculated using the method proposed by Kuang et al. (2017)Kuang et al. (2017).

### 3 Observed simultaneous rapid increase of HONO, nitrate and sulfate

The time series of HONO, sulfate, nitrate and ammonium and precursor gases, meteorological parameters and other parameters are shown in Fig. 2. During this observation period, HONO concentration ranged from 0.31 to 17.6 ppb (ranged from 0.3 to 6.0 ppb during most periods) with an average of 3.0 ppb. The HONO/NO<sub>2</sub> ratio ranged from 0.03 to 0.75 with an average of 0.18, which is higher than the average HONO/NO<sub>2</sub> ratio previously observed in China (Liu et al., 2014; Cui et al., 2018). NO<sub>2</sub> concentration ranged from 7.5 to 60.1 ppb with an average of 32.0 ppb. NH<sub>3</sub> concentration ranged from 0.05 to 30 ppb with an average of 12.3 ppb. Four rapid HONO formation events were identified in Fig. 2, two under foggy conditions and the other two under high RH conditions.

#### 3.1 Explosive growth of HONO during fog episodes

Two dense fog episodes with rapid HONO increase were observed for the first time in China, occurring on the 4<sup>th</sup> and 5<sup>th</sup> Nov. 2016. From satellite images (Fig. 1) it can be seen that on the 5<sup>th</sup> Nov., a wide area of the NCP was shrouded by fog before noon (about 11:30) including the observation site, however, the fog area reduced in the afternoon (about 13:30) and dissipated near the observation site. The evolution of the fog-shrouded area during these two days was also observed by a geostationary satellite (<http://www.eorc.jaxa.jp/ptree/index.html>). These two fog episodes offer us a great opportunity to study the hydrolysis process of NO<sub>2</sub> (R2) and the role of SO<sub>2</sub> in heterogeneous HONO production in fog water (R1), which usually show pH above 5.5 (Safai et al., 2008; Lu et al., 2010).

The time series of simultaneously observed meteorological parameters, concentrations of nitrate, ammonium, sulfate and their precursor gases SO<sub>2</sub>, NO<sub>2</sub>, NO and NH<sub>3</sub>, as well as atmospheric oxidants such as O<sub>3</sub>, H<sub>2</sub>O<sub>2</sub> and other parameters including CO, which is indicative of transport processes during the two days with fog episodes are shown in Fig. 3. From 0:00 (Beijing local time) on the 4<sup>th</sup> Nov., the ambient RH continuously increased and reached 100% near 5:00, and lasted about 8.5 hours before it dropped below 100% near 13:30. However, at 15:30, the ambient RH began to rise again and reached 100% near 19:30, and then sustained until 12:00 on the 5<sup>th</sup> Nov. The latter fog episode lasted about 18.5 hours.

During the first fog episode, the rapid increases of HONO, nitrate, sulfate and ammonium were observed from 8:50 to 11:30 (Case1). HONO increased from 3.6 ppb to 10.6 ppb, with the

most rapid increase occurring around 11:00 at a rate of  $5.5 \text{ ppb h}^{-1}$ . During the HONO increasing period, the variation characteristics of related trace gases and other parameters are as follows.  $\text{NH}_3$  concentration increased slowly at first and then increased drastically near 11 am ( $10 \text{ ppb h}^{-1}$ ).  $\text{SO}_2$  concentration remained almost constant at first and then increased from near 0.25 ppb to 0.4 ppb.  $\text{NO}_2$  concentration increased continuously with a small magnitude, while NO concentration increased first and then decreased.  $\text{H}_2\text{O}_2$  concentration is continuously increasing, but  $\text{O}_3$  concentration remained near zero. CO concentration remained almost constant ( $\sim 2.5 \text{ ppm}$ ), suggesting that there was no evident plume transport during this process. Wind speed was less than  $2 \text{ m s}^{-1}$ , and dropped almost to  $0 \text{ m s}^{-1}$  when HONO concentration dramatically increased, further supporting the fact that the drastic increase was not caused by transport processes. Ammonium, nitrate and sulfate concentration steadily increased from  $40.7, 5.13, 2.13 \text{ } \mu\text{g m}^{-3}$  to  $20.5, 14.3, 30.4, 31.0, 7.9 \text{ ppb } \mu\text{g m}^{-3}$ , respectively. A noticeable increase in nitrite was also observed, when HONO increased most rapidly. It should be noted that the cutting diameter of the IGAC instrument is  $2.5 \text{ } \mu\text{m}$ , which means that observed concentrations only represent the variation of inorganics ions in aerosol water, and that of fog droplets were not included.

During the second fog episode, HONO, nitrate, sulfate and ammonium started to increase rapidly from 9:30 and reached a plateau near 12:30, when the fog started to dissipate (Case2). HONO increased from 3 ppb to 9.5 ppb, with the fastest increase occurring near 11:00 at a rate of  $3.5 \text{ ppb h}^{-1}$ . Variation characteristics of other parameters are as follows.  $\text{NH}_3$  concentration increased steadily from 5 ppb to 24 ppb.  $\text{SO}_2$  concentration increased steadily from 0.25 ppb to 1.25 ppb.  $\text{NO}_2$  concentration remained almost constant at the very beginning (near 40 ppb) and then increase slightly, while NO concentration remained almost constant (near 30 ppb) throughout the entire fog period.  $\text{H}_2\text{O}_2$  concentration increased slightly at first and then rose rapidly towards the end of the fog period.  $\text{O}_3$  concentration increased very slightly. CO concentration remained also near constant ( $\sim 3 \text{ ppm}$ ). Wind speed was steady and less than  $2 \text{ m s}^{-1}$  at the beginning, however, began to increase quickly at noon. Ammonium, nitrate and sulfate concentration steadily grew from  $11.7, 6.7, 8.1, 17, 3.8 \text{ ppb } \mu\text{g m}^{-3}$  to  $22.15, 53.39, 3, 8 \text{ ppb } \mu\text{g m}^{-3}$ , respectively. The variation of nitrite was very similar to that of HONO. The variation of wind speed demonstrate that at the very beginning of the HONO increase, the air mass was relatively stagnant, but became windy when the fog dissipated.

设置了格式: 上标

设置了格式: 上标

设置了格式: 上标

### 3.2 Explosive growth of HONO during haze episodes with high RH conditions

The two periods with rapid HONO increase under high RH conditions occurred on the 11<sup>th</sup> and 14<sup>th</sup> Nov., respectively. The time series of simultaneously observed meteorological parameters, concentrations of nitrate, ammonium, sulfate and their precursor gases SO<sub>2</sub>, NO<sub>2</sub>, NO and NH<sub>3</sub>, as well as oxidants including O<sub>3</sub>, H<sub>2</sub>O<sub>2</sub> and other parameters such as CO concentration, aerosol volume concentration in dry state and aerosol liquid water content during the two days are shown in Fig.4.

On the 11<sup>th</sup> Nov., HONO started rising from 6:30 (3.4 ppb) and came to a halt at 9:00 (11.5 ppb) (Case 3). The quickest increase of HONO occurred near 9 o'clock with a rate of 5.6 ppb<sub>h<sup>-1</sup></sub>. The key features of other parameters are introduced in the following. The ambient RH decreased rapidly (from foggy condition to near 75%). NH<sub>3</sub> increased slowly at first and then grew rapidly. NO<sub>2</sub> increased slowly and SO<sub>2</sub> remained low. The total volume concentration of PM<sub>2.5</sub> was decreasing. Ammonium, nitrate and sulfate concentrations increased very slowly at first and then evident increase was observed in ammonium and nitrate. The decrease in dry state volume concentration of PM<sub>2.5</sub> demonstrate that the air mass is not quite steady due to transport or boundary layer processes. The slight increase of nitrate and sulfate despite the drop in total PM<sub>2.5</sub> concentration suggest that the nitrate and sulfate produced during the increasing process of HONO outgrew those lost to boundary layer mixing and transport.

On the 14<sup>th</sup> Nov., HONO increased drastically near 11:00, reaching 17.6 ppb at 11:30 (16.1 ppb<sub>h<sup>-1</sup></sub>) and then dropped promptly to 4 ppb at 12:30 (Case 4). This phenomenon took place when the fog dissipated and the ambient RH abruptly dropped to near 85%. Key variation features of other parameters are as follows. NH<sub>3</sub> increased rapidly from 9.7 ppb to 30 ppb. NO<sub>2</sub> concentration was increasing quickly, while SO<sub>2</sub> concentration remained low. The concentration of sulfate and nitrate also increased quickly. Volume concentration of PM<sub>2.5</sub> was decreasing, indicating that even more sulfate and nitrate were formed than the observed growth in their concentrations. ~~The O<sub>3</sub> concentration stayed near zero, which means that UV radiation was weak. After the quick formation of HONO, O<sub>3</sub> concentration began to rise, indicating the increase in UV radiation intensity.~~ The photolysis of HONO was high probably the cause for its drastic decrease. Note that the HONO was not increasing during the period where only NO<sub>2</sub> increased rapidly and NH<sub>3</sub> varied little.

设置了格式: 非上标/下标



## 4 Discussions

### 4.1 Discussions on the HONO formation mechanism budget analysis

In these four rapid HONO increasing episodes, the maximum HONO growth rates ( $d[HONO]/[HONO]/dt$ ) all exceed  $5 \text{ ppb}/h$ , and even reach beyond  $16 \text{ ppb}/h$ . Such high HONO growth rates as observed in this study were not yet reported in literature.

The homogeneous reaction of NO with OH is an important source of HONO. In this section, we discuss whether these HONO formation events can be explained by current known mechanisms and which mechanisms are determining the variation of HONO.

The net HONO production rate can be estimated by accounting for all the currently known sources and sinks using the following equation:

$$P_{HONO}^{net} = P_{emi} + P_{hom}^{net} + P_{het} - L_{pho} - L_{dep} \quad (\text{Eq.1})$$

where  $P_{emi}$  is the total emission rate of HONO,  $P_{hom}^{net}$  the net HONO production in homogenous gas phase reactions,  $P_{het}$  the HONO produced via heterogeneous reactions,  $L_{pho}$  the loss of HONO due to photolysis and  $L_{dep}$  the loss of HONO due to deposition.

Previous studies have shown that HONO can be emitted through biomass burning and vehicles (Nie et al., 2015; Huang et al., 2017). Biomass burning contributes to HONO mainly by increasing particle surface area and  $\text{NO}_2$  conversion efficiency (Nie et al., 2015). Under foggy conditions, surface area was not the limiting factor to the  $\text{NO}_2$  conversion. During the haze events, particle surface area was decreasing due to decreasing humidity and aerosol water content. Hence, the variation of surface area cannot explain the observed HONO increases. According to the mapped fire spots on the days of the HONO events (Fig.S3), there was no fire within 20 km distance to the site.  $\text{K}^+$  is often used as an indicator for biomass burning. The average  $\text{K}^+$  concentration during the whole campaign ranged from  $0.022$  to  $5.95 \mu\text{g m}^{-3}$ , with an average of  $1.28 \mu\text{g m}^{-3}$ . The  $\text{K}^+$  level during the four events were  $1.39$ ,  $1.08$ ,  $1.51$  and  $1.54 \mu\text{g m}^{-3}$ , respectively, showing no evident sign of biomass burning. Hence, only vehicle emissions were considered in this study.

Vehicle emissions can be estimated using the following equation:

$$P_{vehicle} = R_{emission} \times [\text{NO}_x]_{vehicle} \quad (\text{Eq.2})$$

where  $R_{emission}$  is the vehicle emission ratio and  $[\text{NO}_x]_{vehicle}$  the  $\text{NO}_x$  concentration from vehicle emissions. The NO/NO<sub>x</sub> ratio during the HONO increasing episodes ranged from 0.37 to 0.76.

带格式的: 缩进: 首行缩进: 0 厘米

设置了格式: 下标

设置了格式: 上标

suggesting that the air masses were relatively aged compared to freshly emitted air mass from exhaust ( $\text{NO}/\text{NO}_x > 0.9$ ).  $P_{\text{vehicle}}^{\text{net}}$  Here,  $P_{\text{vehicle}}$  is estimated assuming all the measured  $\text{NO}_x$  came from vehicle emissions and an emission ratio of 1%, which is higher than the upper limit of 0.8% used in Huang et al. (2017), to obtain an upper limit for vehicle emissions.

HONO can be formed in gas phase reactions of NO with OH radicals and is lost through direct reactions with OH radicals. The net production of HONO via homogeneous reactions can be estimated using the equation:

$$P_{\text{hom}}^{\text{net}} = k_{\text{NO}+\text{OH}}[\text{NO}][\text{OH}] - k_{\text{HONO}+\text{OH}}[\text{HONO}][\text{OH}], \quad (\text{Eq. 4-3})$$

where  $k_{\text{NO}+\text{OH}}$  ( $7.2 \times 10^{-12} \text{ cm}^3 \text{ s}^{-1}$ ) and  $k_{\text{HONO}+\text{OH}}$  ( $5.0 \times 10^{-12} \text{ cm}^3 \text{ s}^{-1}$ ) are the rate constants of the reactions of NO and HONO with OH, at 298 K, respectively (Li et al., 2012).

Using an OH concentration of  $1 \times 10^6 \text{ cm}^{-3}$ , typical for noontime haze conditions, the estimated homogeneous production rate are 2.04, 0.79, 0.33 and 0.37 ppb/h for the episodes on 4<sup>th</sup>, 5<sup>th</sup>, 11<sup>th</sup> and 14<sup>th</sup> Nov., respectively, showing little variability or decreases during the increase of HONO. Clearly, homogeneous oxidation of NO cannot explain the observed HONO variations. The diurnal variation of OH concentrations was inferred from Whalley et al. (2015), replacing OH under fog conditions with  $1 \times 10^5 \text{ cm}^{-3}$ .

Heterogeneous conversion of  $\text{NO}_2$  on aerosol and ground surface is considered a major source for HONO. However, the detailed mechanism (R1 or R2?) is still under debate and different studies have shown a large variability in the range of estimated  $\text{NO}_2$  uptake coefficient. Typically, the conversion of  $\text{NO}_2$  on aerosol and ground surface is parameterized as a linear function of  $\text{NO}_2$  uptake coefficients and surface to volume ratios (surface area densities) (Xue et al., 2014; Li et al., 2018b):

$$P_{\text{het}} = (k_g + k_a)[\text{NO}_2], \quad (\text{Eq.4-1})$$

$$k_g = \frac{1}{8} \cdot \bar{v}_{\text{NO}_2} \cdot \gamma_g \cdot \frac{S}{V}, \quad (\text{Eq.4-2})$$

$$k_a = \frac{1}{4} \cdot \bar{v}_{\text{NO}_2} \cdot \gamma_a \cdot S_a, \quad (\text{Eq.4-3})$$

where  $\bar{v}_{\text{NO}_2}$  stands for the mean molecular speed,  $\gamma_g$  and  $\gamma_a$  for the uptake coefficient on ground and aerosol surface,  $S/V$  for the surface to volume ratio and  $S_a$  for the ambient aerosol surface area density. For  $\text{NO}_2$  conversion on ground surface,  $\gamma_g$  is assumed to be  $1 \times 10^{-6}$  during nighttime and  $2 \times 10^{-5}$  during daytime and  $S/V$  is assumed to be  $0.1 \text{ m}^{-1}$  as in Vogel et al. (2003). Since no measurements of fog droplet surface areas were made in this experiment, we use a  $\gamma_a$  range of

设置了格式: 上标

设置了格式: 上标

$1 \times 10^{-4}$  to  $1 \times 10^{-3}$  as suggested by Li et al. (2018b) and a wide range of surface area densities to account for both aerosol and fog conditions. Additionally, for non-fog conditions, the ambient aerosol surface area density calculated using the simultaneously measured PNSD and aerosol hygroscopicity parameter derived from measurements of a humidified nephelometer system and  $\gamma_a = 1 \times 10^{-4}$  is applied to further calculate the variation of the HONO production on aerosol surface.

HONO loss through photolysis reactions were calculated as:

$$L_{pho} = J_{HONO}[HONO], \quad (\text{Eq.5})$$

where  $J_{HONO}$  was modelled using the TUV radiative transfer model (version 5.3, <http://www2.acom.ucar.edu/modeling/tuv>). The required single scattering albedo and aerosol angstrom exponent were estimated using simultaneously measured PNSD and BC measurements (Kuang et al., 2015), while the 550nm aerosol optical depth (AOD) was assumed to vary with RH (Table S1).

Loss through dry deposition was estimated using equation 6:

$$L_{dep} = \frac{v_{dep}}{H}[HONO], \quad (\text{Eq.6})$$

where the dry deposition rate  $v_{dep}$  was assumed to be  $0.3 \text{ cm s}^{-1}$  according to (Stutz et al., 2002) and the boundary layer height  $H$  was interpolated from ECWMF ERA-interim data (<http://apps.ecmwf.int/datasets/data/interim-full-daily/>).

The comparison between the calculated HONO net production rate and actually measured HONO variation rate ( $d[HONO]/dt$ ) is displayed in Fig. 5. The estimated upper limit for vehicle emissions displays little variability during the day, with slight decreasing trends during the four events, proving that the observed HONO production could not have been caused by direct vehicle emissions. The net gaseous phase production of HONO ( $P_{hom}^{net}$ ) contributed 0.15-0.18, 0.04-0.07, 0.27-1.04 and 0.25-1.53  $\text{ppb h}^{-1}$  during the 4 case events, displaying little influence during fog events and more during haze events. However, the estimated  $P_{hom}^{net}$  was far from sufficient to explain the observed  $d[HONO]/dt$ . Dry deposition was typically high during the night within the shallow nocturnal boundary layer and decreased during the day with the increase of the boundary layer height. The calculated  $L_{dep}$  contributed 0.5-0.9, 0.4-0.6, 2.7-4.3 and 0.05-0.3  $\text{ppb h}^{-1}$  to the loss of HONO. No significant decreases in  $L_{dep}$  were observed during the two fog events, while increases were detected during the cases on 11<sup>th</sup> and 14<sup>th</sup> Nov. Not only was the variation in  $L_{dep}$  unable to explain observed HONO productions, it further added to the discrepancy between observed and calculated  $d[HONO]/dt$ . During the four case events the  $J_{HONO}$  respectively increased

from  $0.7 \times 10^{-4}$  to  $2.5 \times 10^{-4} \text{ s}^{-1}$ ,  $1.6 \times 10^{-4}$  to  $2.4 \times 10^{-4} \text{ s}^{-1}$ ,  $0.03 \times 10^{-4}$  to  $1.4 \times 10^{-4} \text{ s}^{-1}$  and  $1.6 \times 10^{-4}$  to  $4.4 \times 10^{-4} \text{ s}^{-1}$ , with  $L_{pho}$  contributing 0.9-8.9, 2.2-7.8, 0.03-5.5 and 0.8-26.4 ppb h<sup>-1</sup> to the loss of HONO.  $J_{HONO}$  increased significantly by the end of the HONO growth events to  $2.9 \times 10^{-4}$ ,  $4.3 \times 10^{-4}$ ,  $2.6 \times 10^{-4}$  and  $6.6 \times 10^{-4} \text{ s}^{-1}$ , respectively, suggesting that the rapid drop of HONO concentrations was high probably caused by the rapid photolysis. Overall,  $L_{pho}$  contributed most to the discrepancy between observed and calculated d[HONO]/dt.

Generally, the observed and calculated d[HONO]/dt agreed better with each other outside the HONO explosive growth periods, showing overestimations when aerosol liquid water contents were high, suggesting possible overestimation in the NO<sub>2</sub> uptake coefficient in the parameterization of  $P_{het}$ . This further suggests that the observed discrepancies in HONO production have mainly been caused by uncertainties in the heterogeneous formation estimates. ~~The NO/NO<sub>x</sub> ratio during the HONO increasing episodes ranged from 0.37 to 0.76, suggesting that the air masses were relatively aged compared to freshly emitted air mass from exhaust (NO/NO<sub>x</sub> > 0.9). Even if we assume all the measured NO<sub>x</sub> came from vehicle emissions and an emission ratio of 10%, which is higher than the upper limit of 8% used in Huang et al. (2017) (Huang et al., 2017), the contribution of vehicle emissions to HONO would be in the range of 0.97 to 1.09, 0.63 to 0.83, 0.73 to 1.16 and 0.9 to 1.15 ppb during the episodes on 4<sup>th</sup>, 5<sup>th</sup>, 11<sup>th</sup> and 14<sup>th</sup> Nov., respectively. Even if the emission ratio were underestimated, NO<sub>x</sub> decreased during these events with the increase in HONO, which proves that the observed HONO variation could not have been caused by direct vehicle emissions.~~

Recent studies also suggest biomass burning to be an important HONO source, mainly by increasing particle surface area and NO<sub>2</sub> conversion efficiency (Nie et al., 2015). Under foggy conditions, surface area is not the limiting factor to the NO<sub>2</sub> conversion. During the haze events, particle surface area was decreasing due to decreasing humidity and aerosol water content. Hence, the variation of surface area cannot explain the observed HONO increases. According to the mapped fire spots on the days of the HONO events (Fig. S2), there was no fire within 20 km distance to the site. ~~K<sub>2</sub><sup>+</sup> is often used as an indicator for biomass burning. The average K<sub>2</sub><sup>+</sup> concentration during the whole campaign ranged from 0.022 to 5.95 μg/m<sup>3</sup>, with an average of 1.28 μg/m<sup>3</sup>. The K<sub>2</sub><sup>+</sup> level during the four events were 1.39, 1.08, 1.51 and 1.54 μg/m<sup>3</sup>, respectively, showing no evident sign of biomass burning.~~

设置了格式: 下标

设置了格式: 上标

The fact that HONO drastically increased while NO<sub>2</sub> varied little (9:30 to 11:30, 5<sup>th</sup> Nov. and 6:30 to 8:30, 11<sup>th</sup> Nov.) or hardly increased even under drastic increases of NO<sub>2</sub> (8:30 to 11:30, 14<sup>th</sup> Nov.), but displayed explosive growth with increasing NH<sub>3</sub>, ~~cannot~~ could not be explained by current known HONO sources (direct emission or gas phase reactions). ~~These~~ Additionally, these rapid increasing HONO phenomena were all observed under foggy or ~~under~~ high RH conditions, which ~~leads us to suspect~~ further affirms the suspicion that the HONO increase was caused by heterogeneous conversion of NO<sub>2</sub>. ~~Was it R1, R2 or another mechanism that led to the explosive growth of HONO?~~

~~Based on results from Wang et al. (2016a) and Cheng et al. (2016), R1 is more likely to happen during fog episodes or under NH<sub>3</sub> neutralized conditions (3,4). While R1 might be able to explain the formation of sulfate and HONO, it cannot explain that of nitrate. The observed molar increase of nitrate were always larger than that of sulfate, usually exceeding twice the amount of sulfate. In addition, pH values during the rapid HONO increasing period under high RH conditions (estimated from ISORROPIA with the forward mode and metastable assumption (Song et al., 2018), Fig. 4) were continuously below 5, further demonstrating that R1 is unlikely to happen under such conditions.~~

~~Laboratory experiments demonstrated that anions greatly enhance NO<sub>2</sub> uptake on water~~ **4.2**

#### **Heterogeneous HONO formation mechanism**

As manifested in Sect. 4.1, the unknown HONO source and the overestimates in HONO production were both linked to our limited understanding on the heterogeneous HONO formation mechanism. In this section, we try to evaluate the relative contribution of the currently known heterogeneous HONO formation pathways (R1 and R2) and reveal the reason for their limitations in explaining the observed HONO growth.

To evaluate which process (R1 or R2) was dominating the heterogeneous production of HONO, we assume that HONO was produced in aerosol and fog water simultaneously via R1 and R2. Since measurements of fog liquid water content or fog droplet surface area density were not made, we cannot directly quantify the absolute HONO production in fog. However, we can make a few assumptions to compare the relatively HONO contribution via R1 and R2. First, it was assumed that the observed sulfate production ( $d[\text{SVI}]/dt$ ) was caused by the reaction of SO<sub>2</sub> with H<sub>2</sub>O<sub>2</sub>, O<sub>3</sub>, NO<sub>2</sub>, transition metal ions (TMI: Fe<sup>3+</sup> and Mn<sup>2+</sup>). Calculations were performed according to Cheng et al. (2016), using the same pH dependent TMI concentrations and the

actually measured SO<sub>2</sub>, H<sub>2</sub>O<sub>2</sub>, O<sub>3</sub> and NO<sub>2</sub> concentrations (Table S2). For the two fog episodes on 4<sup>th</sup> and 5<sup>th</sup> Nov. 2016, the mean diameter of fog droplets was assumed to be 7.0 μm and the liquid water content was assumed to be 0.3 g m<sup>-3</sup> according to Shen et al. (2018). For the haze episodes on the 11<sup>th</sup> and 14<sup>th</sup> Nov. 2016, the mean aerosol diameter under ambient conditions was estimated to be 0.65-1.22 and 0.9 μm, while the liquid water content was calculated to decrease from 3.4×10<sup>-4</sup> to 7.8×10<sup>-5</sup> g m<sup>-3</sup> on the 11<sup>th</sup> Nov and assumed to be 0.01 g m<sup>-3</sup> on the 14<sup>th</sup> Nov, during the transition from fog to haze. The sulfate production rate and relative contribution of each oxidation pathway to the total sulfate production rate was obtained and depicted in Fig.6. For the two fog episodes, assuming pH=6, the estimated average sulfate production rates are 11.7 and 31.6 μg m<sup>-3</sup> h<sup>-1</sup> approximately 4 times of that observed within PM<sub>2.5</sub>, which might be an underestimation, considering the liquid water content of fog droplets are at least a magnitude higher than that of aerosols. For the two haze episodes, using the pH values estimated using ISORROPIA (forward mode and metastable assumption (Song et al., 2018)), the estimated average sulfate production rates are 0.06 and 1.8 μg m<sup>-3</sup> h<sup>-1</sup>, about 10% of that observed within PM<sub>2.5</sub>. Following the calculations of Cheng et al. (2016), we have considered the influence of ionic strength on the reaction rates and set constraints on the maximum ionic strength (*I*<sub>max</sub>), which might have caused underestimations for all reaction routes, since the calculated ionic strength commonly exceeded *I*<sub>max</sub>. Underestimated transition metal ion concentrations may also be partly responsible for the underpredicted sulfate production, since the TMI catalysis route has recently be pointed out to be the dominant SO<sub>2</sub> heterogeneous oxidation pathway {Shao, 2019 #2155}. Additionally, there also might be other neglected SO<sub>2</sub> oxidation pathways, which will lead to overestimates in the sulfate fraction produced by the NO<sub>2</sub> oxidation pathway. Therefore, we can only yield an upper limit for the HONO production rate of R1:

$$\frac{d[HONO]}{dt}_{R1} = 2 \times frac_{SO_2+NO_2} \times \frac{d[SVI]}{dt}_{obs} \quad (Eq.7)$$

where *frac*<sub>SO<sub>2</sub>+NO<sub>2</sub></sub> is the contribution fraction of the NO<sub>2</sub> oxidation pathway to the total sulfate production. Note that the calculated HONO production rate can only represent the production within PM<sub>2.5</sub>.

By further assuming that all the observed nitrate production ( $d[\text{NO}_3^-]/dt$ ) was caused by reaction R2 and by the reaction of  $\text{NO}_2$  with OH radicals ( $k_{\text{NO}_2+\text{OH}}=3.2\times10^{-12} \text{ cm}^3 \text{ s}^{-1}$ ), the HONO production rate of R2 would be:

$$\frac{d[\text{HONO}]}{dt}_{\text{R2}} = \frac{d[\text{NO}_3^-]}{dt}_{\text{obs}} - k_{\text{NO}_2+\text{OH}}[\text{NO}_2][\text{OH}]. \quad (\text{Eq.8})$$

The contribution fraction of the two reactions to the heterogeneous HONO production in aerosol and fog liquid water content can be calculated by:

$$f_{\text{R1}} = \frac{d[\text{HONO}]}{dt}_{\text{R1}} / \frac{d[\text{HONO}]}{dt}_{\text{R1+R2}} \quad \text{and} \quad (\text{Eq.9-1})$$

$$f_{\text{R2}} = \frac{d[\text{HONO}]}{dt}_{\text{R2}} / \frac{d[\text{HONO}]}{dt}_{\text{R1+R2}}. \quad (\text{Eq.9-2})$$

Assuming the pH of fog droplets falls within the range of 4 to 6,  $f_{\text{R2}}$  was estimated to range from 75.5 to 99.5% and from 81.2 to 99.5% during the 4<sup>th</sup> and 5<sup>th</sup> Nov. 2016, respectively. For the two haze events on 11<sup>th</sup> and 14<sup>th</sup> Nov., the  $f_{\text{R2}}$  corresponding to the pH values modelled by ISORROPIA would be 98.2% and 97.3%.

These results suggest that, reaction R2 is the dominant contributor to the heterogeneous HONO production, while R1 is more important under high pH conditions. Under the assumed upper limit of pH, R1 can contribute up to 24.5%, 18.8% to the observed HONO growth during the fog events. This is in accordance with results from (Yabushita Wang et al., 2009; Li et al., 2018b, 2016), which suggests that R2 is more likely to occur in fog water that is rich in anions. The concentration of  $\text{NO}_2$  as well as the surface area density of fog droplets should be and Cheng et al. (2016), which suggested that R1 was more likely to happen during fog episodes or under  $\text{NH}_3$  neutralized conditions (3,4). For the two haze events, R1 contributed very little (1.8% and 2.7%) to the observed HONO growth.

Since R2 seems to be the dominant contributor to the observed HONO production, it is important to evaluate whether the parameterizations in current literature can accurately describe the HONO production process of R2. The HONO production rate of R2 is typically parameterized as in Eq.4, where the  $\text{NO}_2$  concentration and the surface area density of fog droplets/aerosol particles are the controlling factors of the  $\text{NO}_2$  uptake, as opposed to the pH of the water droplets- (Li et al., 2018b; Yabushita et al., 2009). Based on the reactive uptake coefficient of  $\text{NO}_2$  ( $\gamma_{\text{NO}_2}$ ) in Yabushita et al. (2009), we have in Yabushita et al. (2009) and Li et al. (2018b), we have calculated

the HONO production rate of R2 under different conditions (see Fig. S4). During foggy conditions, the HONO production rate should be higher than  $1 \text{ ppb} / (\text{ppb} \cdot \text{NO}_2 \cdot \text{h})^{-1}$ . The  $\text{NO}_2$  concentration during the two fog episodes ranged between 40 to 50 ppb, therefore, the HONO production rate ~~should be~~ would have been higher than 40 ppb/h during the observed fog periods according to the results in Fig. S1. However, no rapid increase of HONO was observed unless  $\text{NH}_3$  was simultaneously increasing. This result indicates As already mentioned before, under hazy conditions,  $P_{\text{het}}$  significantly overestimated the HONO production when relative humidity was high and large ambient aerosol surface area densities were observed (Fig5), while it failed to reproduce the growth in HONO on the morning of the 11<sup>th</sup> Nov. 2016. These results indicate that R2 is missing the important impact of  $\text{NH}_3$  in the heterogeneous HONO production and that the currently used  $\gamma_{\text{NO}_2}$  range is at least overestimated when  $\text{NH}_3$  is not abundant enough.

Recent theoretical simulation results (Li et al., 2018a) ascertain that  $\text{NH}_3$  can promote the hydrolysis of  $\text{NO}_2$  and contribute to HONO formation via R2 (Li et al., 2018a). This conclusion is consistent with the observed phenomena that HONO only increased rapidly when  $\text{NH}_3$  was simultaneously increasing. Considering the influence of  $\text{NH}_3$  and sulfate on the aerosol pH, under our observed  $\text{NH}_3$  concentration range,  $\text{NH}_3$  has negligible impact on pH values (Guo et al., 2017), especially under high RH conditions. This further proves that the  $\text{NH}_3$ -promoted hydrolysis of  $\text{NO}_2$  is independent of the pH value.

~~So what role does  $\text{SO}_2$  play in the HONO formation and what caused the rapid formation of sulfate? Li et al. (2018b) pointed out that  $\text{NO}_2$  can oxidize S(IV) indirectly via free radical mechanism (the involved reactions RS1 to RS5 proposed in Li et al. (2018b) are listed in the supplement). The key step of the proposed S(IV) oxidation pathway is the photolysis of HONO to produce OH (RS1). Produced OH can oxidize S(IV) to form bisulfate or sulfate through reaction RS2 and produce  $\text{HO}_2$ .  $\text{HO}_2$  can react with NO to produce  $\text{NO}_2$ , or react with itself to produce  $\text{H}_2\text{O}_2$ . Is the radiation during fog and haze events strong enough to photo dissociate the produced HONO and release large amounts of OH radicals? Diurnal evolutions of the lifetime of HONO (only considering the photolysis process) under different aerosol optical depth (AOD) and different cloud optical depth conditions are presented in Fig.5, which were calculated using the j-values simulated by the TUV radiative transfer model (version 5.3, <http://www2.acom.ucar.edu/modeling/tuv>, the required single scattering albedo and aerosol angstrom exponent were estimated using simultaneously measured PNSD and BC measurements~~



(Kuang et al., 2015). The results in Fig. 5a demonstrate that for AOD (550nm)=1.0, the lifetime of HONO quickly drops below 1 hour after sunrise and is less than 0.5 hour at noontime. The AOD at 550 nm observed near 13:30 by the MODIS (Moderate-resolution Imaging Spectroradiometer) Aqua satellite on the 14<sup>th</sup> November is 0.7, thus, the drastic decrease of HONO on the 14<sup>th</sup> November can be well explained by its rapid photolysis and the amount of OH radicals released must be even greater than the drop in HONO concentrations, since HONO was simultaneously produced via NO<sub>2</sub> hydrolysis. During Case 1 and 3, HONO began to decrease when NH<sub>3</sub> was still increasing. The reason might be that the UV radiation at that point was already strong enough to photolyze HONO quickly, which lead to the drastic drop in HONO concentrations (The diurnal evolution of lifetime of HONO under different cloud optical depth conditions are depicted in Fig. 5b). O<sub>3</sub> started to increase quickly as HONO began to decrease, which is an indirect evidence of the increasing UV radiation. The increase in H<sub>2</sub>O<sub>2</sub> during the increase of HONO in the two fog episodes, where O<sub>3</sub> concentration stayed near zero, might be an indirect evidence of the HO<sub>2</sub> production and occurrence of RS2. The formed H<sub>2</sub>O<sub>2</sub> can also oxidize S(IV) to form sulfate via heterogeneous processes, even more efficient than the OH radical oxidation in the gas phase under high RH conditions. In this way, the simultaneous formation of HONO, sulfate and nitrate can be well explained and it becomes clear that SO<sub>2</sub> does not participate in the heterogeneous HONO production process.

Another phenomenon worth noting is that, in Case 3, HONO was increasing rapidly even under the drastic decrease in ambient RH, which demonstrates that the impact of NH<sub>3</sub> on HONO formation should be even more important than that of aerosol liquid water content. However, the hydrolysis of NO<sub>2</sub> needs water to be involved, thus, the importance of water content under different conditions remains to be elucidated.

To further investigate the acceleration effect of NH<sub>3</sub> on the hydrolysis of NO<sub>2</sub>, we have examined the correlations between the NO<sub>2</sub>-to-HONO (HONO/NO<sub>2</sub> ratio), NO<sub>2</sub>-to-NO<sub>3</sub><sup>-</sup> (NO<sub>3</sub><sup>-</sup>/NO<sub>2</sub> ratio) conversion efficiencies and the NH<sub>3</sub> concentration during the entire field campaign (Fig. 6). Note that only data points during nighttime (18 pm to 6 am) and with ambient RH Higher<sup>higher</sup> than 80% are shown<sup>displayed</sup> in Fig. 6-7. Daytime data were excluded, because HONO would quickly photolyze as soon as sunlight ~~is was~~ available, ~~even~~. Even if there was rapid HONO production, the corresponding increase of HONO might not be ~~observed~~observable due to its quick photolysis. The reason for only including data with ambient RH higher than 80% is

~~because that~~ the quick hydrolysis of NO<sub>2</sub> requires water to be involved. However, the overall hygroscopicity of ambient aerosols during this field campaign ~~is was~~ relatively low ~~with an~~ average hygroscopicity parameter  $\kappa$  ~~is of~~ 0.14, ~~and the volume contribution of liquid water to the total volume concentrations of ambient aerosols was quite low when ambient RH is below 80% (Kuang et al., 2018) and the volume contribution of liquid water to the total volume concentrations of ambient aerosols is quite low when ambient RH is below 80% during this field campaign. Details on the volume contribution of liquid water to the total volume of ambient aerosols can be referred to Kuang et al. (2018).~~ The correlation coefficient between HONO/NO<sub>2</sub> ratio and the NH<sub>3</sub> concentration reaches 0.68, while that between NO<sub>3</sub><sup>-</sup>/NO<sub>2</sub> ratio and NH<sub>3</sub> concentration only reaches 0.48, since the source of NO<sub>3</sub><sup>-</sup> is much more complicated than that of HONO. These results have further verified that NH<sub>3</sub> promotes the NO<sub>2</sub> hydrolysis and HONO production. The correlation of HONO/NO<sub>2</sub> to NH<sub>3</sub> is highly nonlinear, HONO/NO<sub>2</sub> increases rapidly with NH<sub>3</sub> when NH<sub>3</sub> reaches above 10 ppb.

#### **4.2 Diurnal variations of 3 Feedback between HONO formation and inorganic secondary aerosol formation and aerosol hygroscopicity determined by NH<sub>3</sub>**

~~According to the discussions in Sect.4.1, NH<sub>3</sub> promotes the hydrolysis of NO<sub>2</sub>, producing HONO and nitrate. During daytime, HONO photolysis further produces OH and results in significant formation of sulfate. According to the discussions in Sect.4.2, NH<sub>3</sub> promotes the hydrolysis of NO<sub>2</sub>, producing nitrate and most of the observed HONO. However, the connection between the NH<sub>3</sub> promoted hydrolysis and the simultaneous rapid sulfate production remains unexplained. As was already discussed in Sect.4.2, the sulfate production rate calculated based on currently known SO<sub>2</sub> oxidation pathways largely underestimates the observed sulfate growth, indicating that there might be neglected oxidation pathways. Li et al. (2018b) pointed out that NO<sub>2</sub> can oxidize S(IV) indirectly via free radical mechanism (the involved reactions RS1 to RS5 proposed in Li et al. (2018b) listed in the supplement). The key step of the proposed S(IV) oxidation pathway is the photolysis of HONO to produce OH radicals (RS1). OH can oxidize S(IV) to form bisulfate or sulfate through reaction RS2 and produce HO<sub>2</sub>. HO<sub>2</sub> can react with NO to produce NO<sub>2</sub>, or react with itself to produce H<sub>2</sub>O<sub>2</sub>. As was depicted in Fig.5, the radiation during the fog/haze events was already strong enough to photolyze the produced HONO and release OH radicals at the same rates as  $L_{pho}$  in Sect. 4.1, indicating there was strong OH production, especially~~

带格式的: 1 级

near the end of the events. For the two fog events, no AOD measurements were available. Assuming AOD=2.5 for foggy conditions, the lifetime of HONO (only considering the photolysis process) were estimated to decrease from 4.2 to 1.1 h, 1.7 to 1.1 h during the growth of HONO and to drop to 1.0 and 0.7 h by the time of the drastic decreases in HONO. In the haze event on the 11<sup>th</sup> Nov., AOD measurements were also not available due to cloud coverage, however, sensitivity study shows that the calculated HONO lifetime are much more sensitive to the AOD as opposed to the COD values (increasing 3.1 and 0.4 h per 0.1 increase in AOD and COD, Fig.S5). The HONO lifetime dropped from 2.0 h (by the time of the HONO peak) to 1.1 h (by time of the HONO decrease). During the case on the 14<sup>th</sup> Nov, 2016, the relative humidity decreased from 100% (10:00-11:00) to 86% (11:30), suggesting that this was a fog dissipation process. The HONO lifetime was estimated to be 1.7 h between 10:00 to 11:00, proving that the photolysis process was relatively weaker during the rapid increase of HONO. The estimated HONO lifetime rapidly decreased to 0.6 h by 12:00, resulting in accelerated HONO dissociation and OH production. The increase in H<sub>2</sub>O<sub>2</sub> observed during and after the increase of HONO, might be an indirect evidence of the HO<sub>2</sub> production and occurrence of RS2. The observed H<sub>2</sub>O<sub>2</sub> concentrations were much higher than the assumptions of 0.01 ppb made in Cheng et al. (2016), which was also pointed out by Ye et al. (2018). Under the assumed pH range for fog and the calculated pH range for aerosol, the estimated sulfate production was dominated by the SO<sub>2</sub> oxidation via H<sub>2</sub>O<sub>2</sub> (Fig.6). This indicates that both the calculated and the yet unexplained sulfate production were linked to the photolysis of HONO.

NH<sub>3</sub> promoted the hydrolysis of NO<sub>2</sub>, producing HONO and nitrate. HONO easily photolyzes releasing OH radicals, which further converted to HO<sub>2</sub> and H<sub>2</sub>O<sub>2</sub>. The highly oxidative free radicals and H<sub>2</sub>O<sub>2</sub> collaboratively boosted the formation of sulfate. Hence, diurnal variations of NH<sub>3</sub> should have exerted significant influences on the diurnal variations of HONO and inorganic aerosol chemical components- (sulfate, nitrate and ammonium, SNA). The average diurnal variations of NO<sub>2</sub>, NH<sub>3</sub>, HONO as well as SO<sub>2</sub> concentrations during this field campaign are shown in Fig.7a8a. The average HONO concentration during nighttime is higher than that during daytime due to the quick photolysis of HONO upon solar irradiation. The NH<sub>3</sub> concentration begins to increase in the morning (near 8 o'clock:00 LT) the reaches the plateau in the afternoon (8.5 to 15.5 ppb in average), and the SO<sub>2</sub> concentrations shows a similar diurnal variation to that of NH<sub>3</sub>. This type of diurnal variation of SO<sub>2</sub> was also found by Xu et al. (2014), however, the cause of this

common diurnal pattern of between  $\text{NH}_3$  and  $\text{SO}_2$  during this field campaign requires further investigation. The  $\text{NO}_2$  concentration increases quickly in the afternoon and decreases in the evening.

As shown in Fig. 7b8b, the increase of  $\text{NH}_3$  from morning to the afternoon was accompanied with the increase of mass fractions of nitrate and sulfate in  $\text{PM}_{2.5}$  (The mass fractions of different aerosol chemical compositions were obtained by using the measured dry state PNSD to calculate volume concentration of  $\text{PM}_{2.5}$ , assuming that the density of aerosols in dry state is  $1.5 \text{ g/cm}^3$  (Yin et al., 2015). The results shown in Fig. 7b8b indicate that the molecular concentration increase in nitrate from the morning and to the afternoon is much faster than that of sulfate, since the molar mass of sulfate is much higher than that of nitrate, again supporting the theory of fact that the  $\text{NH}_3$ -promoted  $\text{NO}_2$  hydrolysis, which only produces HONO and nitrate directly. It is noteworthy that, in the morning, was the main contributor to the observed explosive HONO formation. The evident morning increase of the contribution of inorganic aerosol components (sulfate, nitrate, ammonium) to ambient aerosol mass component fractions resulted in prominent increases of aerosol hygroscopicity, displaying an average hygroscopicity parameter  $\kappa$  anomaly of +0.04 during this field campaign is 0.14 (Kuang et al., 2017) as shown in noontime (Fig. 7e-8c). From the morning to the afternoon, the ambient RH decreases quickly, however, the increase of aerosol hygroscopicity will can retard the decrease of aerosol liquid water content and surface area density of ambient aerosols. This This might acts as a positive feedback, further enhances enhancing the hydrolysis of  $\text{NO}_2$  as well as the nitrate and sulfate formation as opposed to conditions with constant aerosol hygroscopicity.

## 5. Summary and atmospheric implications

Explosive HONO growth (observed maximum  $d[\text{HONO}]/d[\text{HONO}]/dt = 16.1 \text{ ppb/h}^{-1}$ ) was observed for the first time on the NCP during fog and haze episodes with high RH conditions, only occurring with evident increases in  $\text{NH}_3$ , indicating that  $\text{NH}_3$  is the key factor promoting the hydrolysis of  $\text{NO}_2$ , resulting in rapid HONO and nitrate formation.  $\text{NH}_3$  concentrations during the observation period exhibit a distinct diurnal variation with an increase in the morning and a peak in the afternoon (8.5 to 15.5 ppb in average). The increase of  $\text{NH}_3$  promotes the hydrolysis of  $\text{NO}_2$ , giving significant rise to HONO and nitrate concentrations. Produced HONO released OH radicals upon photolysis, which further oxidized  $\text{SO}_2$  to sulfate through gas phase and heterogeneous reactions. Therefore, the significant diurnal variations growth

带格式的: 1 级

of NH<sub>3</sub> ~~has in the morning~~ determined the ~~diurnal variations of increase in~~ nitrate, sulfate and ammonium as well as that of aerosol hygroscopicity, ~~which as a positive feedback retards the decrease in atmospheric liquid water content and further enhances the hydrolysis of NO<sub>2</sub> as well as the nitrate and sulfate formation.~~

Results in this paper reveals that the NH<sub>3</sub>-promoted NO<sub>2</sub> hydrolysis is a significant source of HONO, which provides direct insight into the missing daytime source of HONO on the NCP. Results in this paper also shed light on the recent controversy of how SO<sub>2</sub>, pH and NH<sub>3</sub> are involved in heterogeneous HONO production. It was clarified that ~~SO<sub>2</sub> does not directly take part in the~~ HONO production, ~~but is~~ SO<sub>2</sub> took a minor part during fog events and an insignificant part during haze events, the observed growth in sulfate was dominantly the byproduct of the HONO photolysis, confirming again the importance HONO as an OH source and its crucial role in atmospheric chemistry.

These results have demonstrated the critical role and contribution of NH<sub>3</sub> in the formation of photochemical and aerosol pollution on the North China Plain. Effective control measures are urgently called for to reduce NH<sub>3</sub> emissions, which would simultaneously benefit the photochemical and aerosol pollution abatement through the reduction of HONO production.

#### Acknowledgments, Samples, and Data

This work is supported by the National Key R&D Program of China (2016YFC0202300), the National research program for key issues in air pollution control (DQGG0103) and the National Natural Science Foundation of China (41505107 and 41590872). We thank Wei Peng from Beijing Met High-Tech Co., Ltd. for his help with the maintenance of the IGAC instrument.

**Data availability.** The data used in this study are available from the corresponding author upon request (kuangye@jnu.edu.cn)

#### References

- Cheng, Y., Zheng, G., Wei, C., Mu, Q., Zheng, B., Wang, Z., Gao, M., Zhang, Q., He, K., Carmichael, G., Pöschl, U., and Su, H.: Reactive nitrogen chemistry in aerosol water as a source of sulfate during haze events in China, *Science Advances*, 2, [e1601530](#), 10.1126/sciadv.1601530, 2016.
- Cui, L., Li, R., Zhang, Y., Meng, Y., Fu, H., and Chen, J.: An observational study of nitrous acid (HONO) in Shanghai, China: The aerosol impact on HONO formation during the haze episodes, *The Science of the total environment*, 630, 1057-1070, 10.1016/j.scitotenv.2018.02.063, 2018.
- Ding, J., Zhao, P., Su, J., Dong, Q., and Du, X.: Aerosol pH and its influencing factors in Beijing, *Atmos. Chem. Phys. Discuss.*, 2018, 1-34, 10.5194/acp-2018-270, 2018.

带格式的: 两端对齐

Guo, H., Weber, R. J., and Nenes, A.: High levels of ammonia do not raise fine particle pH sufficiently to yield nitrogen oxide-dominated sulfate production, *Scientific reports*, 7, 12109, 10.1038/s41598-017-11704-0, 2017.

Huang, R.-J., Yang, L., Cao, J., Wang, Q., Tie, X., Ho, K.-F., Shen, Z., Zhang, R., Li, G., Zhu, C., Zhang, N., Dai, W., Zhou, J., Liu, S., Chen, Y., Chen, J., and O'Dowd, C. D.: Concentration and sources of atmospheric nitrous acid (HONO) at an urban site in Western China, *Science of The Total Environment*, 593-594, 165-172, <https://doi.org/10.1016/j.scitotenv.2017.02.166>, <https://doi.org/10.1016/j.scitotenv.2017.02.166>, 2017.

Kleffmann, J., Gavriloaiei, T., Hofzumahaus, A., Holland, F., Koppmann, R., Rupp, L., Schlosser, E., Siese, M., and Wahner, A.: Daytime formation of nitrous acid: A major source of OH radicals in a forest, *Geophysical Research Letters*, 32, doi:10.1029/2005GL022524, 2005.

Kuang, Y., Zhao, C. S., Tao, J. C., and Ma, N.: Diurnal variations of aerosol optical properties in the North China Plain and their influences on the estimates of direct aerosol radiative forcing, *Atmos. Chem. Phys. Discuss.*, 15, 339-369, 10.5194/acpd-15-339-2015, 2015.

Kuang, Y., Zhao, C., Tao, J., Bian, Y., Ma, N., and Zhao, G.: A novel method for deriving the aerosol hygroscopicity parameter based only on measurements from a humidified nephelometer system, *Atmos. Chem. Phys.*, 17, 6651-6662, 10.5194/acp-17-6651-2017, 2017.

Kuang, Y., Zhao, C. S., Zhao, G., Tao, J. C., Xu, W., Ma, N., and Bian, Y. X.: A novel method for calculating ambient aerosol liquid water content based on measurements of a humidified nephelometer system, *Atmospheric Measurement Techniques*, 11, 2967-2982, 10.5194/amt-11-2967-2018, 2018.

Li, L., Duan, Z., Li, H., Zhu, C., Henkelman, G., Francisco, J. S., and Zeng, X. C.: Formation of HONO from the NH<sub>3</sub>-promoted hydrolysis of NO<sub>2</sub>-dimers in the atmosphere, *Proceedings of the National Academy of Sciences*, 10.1073/pnas.1807719115, 2018a.

Li, L., Hoffmann, M. R., and Colussi, A. J.: Role of Nitrogen Dioxide in the Production of Sulfate during Chinese Haze-Aerosol Episodes, *Environmental science & technology* *Science & Technology*, 52, 2686-2693, 10.1021/acs.est.7b05222, 2018b.

Li, X., Brauers, T., Häseler, R., Bohn, B., Fuchs, H., Hofzumahaus, A., Holland, F., Lou, S., Lu, K. D., Rohrer, F., Hu, M., Zeng, L. M., Zhang, Y. H., Garland, R. M., Su, H., Nowak, A., Wiedensohler, A., Takegawa, N., Shao, M., and Wahner, A.: Exploring the atmospheric chemistry of nitrous acid (HONO) at a rural site in Southern China, *Atmospheric Chemistry and Physics*, 12, 1497-1513, 10.5194/acp-12-1497-2012, 2012.

Liu, M., Song, Y., Zhou, T., Xu, Z., Yan, C., Zheng, M., Wu, Z., Hu, M., Wu, Y., and Zhu, T.: Fine particle pH during severe haze episodes in northern China, *Geophysical Research Letters*, 44, 5213-5221, doi:10.1002/2017GL073210, 2017a.

Liu, Y., Wu, Z., Wang, Y., Xiao, Y., Gu, F., Zheng, J., Tan, T., Shang, D., Wu, Y., Zeng, L., Hu, M., Bateman, A. P., and Martin, S. T.: Submicrometer Particles Are in the Liquid State during Heavy Haze Episodes in the Urban Atmosphere of Beijing, China, *Environmental Science & Technology Letters*, 4, 427-432, 10.1021/acs.estlett.7b00352, 2017b.

Liu, Z., Wang, Y., Costabile, F., Amoroso, A., Zhao, C., Huey, L. G., Stickel, R., Liao, J., and Zhu, T.: Evidence of Aerosols as a Media for Rapid Daytime HONO Production over China, *Environmental science & technology* *Science & Technology*, 48, 14386-14391, 10.1021/es504163z, 2014.

682 Lu, C., Niu, S., Tang, L., Lv, J., Zhao, L., and Zhu, B.: Chemical composition of fog water in  
683 Nanjing area of China and its related fog microphysics, *Atmospheric Research*, 97, 47-69,  
684 <http://dx.doi.org/10.1016/j.atmosres.2010.03.007>, 2010.

685 Lu, K., Guo, S., Tan, Z., Wang, H., Shang, D., Liu, Y., Li, X., Wu, Z., Hu, M., and Zhang, Y.:  
686 Exploring atmospheric free-radical chemistry in China: the self-cleansing capacity and the  
687 formation of secondary air pollution, *National Science Review*, nwy073-nwy073,  
688 10.1093/nsr/nwy073, 2018.

689 [Meng, Z., Xu, X., Lin, W., Ge, B., Xie, Y., Song, B., Jia, S., Zhang, R., Peng, W., Wang, Y.,](#)  
690 [Cheng, H., Yang, W., and Zhao, H.: Role of ambient ammonia in particulate ammonium formation](#)  
691 [at a rural site in the North China Plain, \*Atmos. Chem. Phys.\*, 18, 167-184, 10.5194/acp-18-167-](#)  
692 [2018, 2018.](#)

693 Michoud, V., Colomb, A., Borbon, A., Miet, K., Beekmann, M., Camredon, M., Aumont, B.,  
694 Perrier, S., Zapf, P., Siour, G., Ait-Helal, W., Afif, C., Kukui, A., Furger, M., Dupont, J. C.,  
695 Haefelin, M., and Doussin, J. F.: Study of the unknown HONO daytime source at a European  
696 suburban site during the MEGAPOLI summer and winter field campaigns, *Atmos. Chem. Phys.*,  
697 14, 2805-2822, 10.5194/acp-14-2805-2014, 2014.

698 Nie, W., Ding, A. J., Xie, Y. N., Xu, Z., Mao, H., Kerminen, V. M., Zheng, L. F., Qi, X. M., Huang,  
699 X., Yang, X. Q., Sun, J. N., Herrmann, E., Petäjä, T., Kulmala, M., and Fu, C. B.: Influence of  
700 biomass burning plumes on HONO chemistry in eastern China, ~~*Atmospheric Chemistry and*~~  
701 ~~*Physics*~~, *Atmos. Chem. Phys.*, 15, 1147-1159, 10.5194/acp-15-1147-2015, 2015.

702 Petters, M. D., and Kreidenweis, S. M.: A single parameter representation of hygroscopic growth  
703 and cloud condensation nucleus activity, *Atmospheric Chemistry and Physics*, 7, 1961-1971, 2007.

704 Ran, L., Zhao, C. S., Xu, W. Y., Lu, X. Q., Han, M., Lin, W. L., Yan, P., Xu, X. B., Deng, Z. Z.,  
705 Ma, N., Liu, P. F., Yu, J., Liang, W. D., and Chen, L. L.: VOC reactivity and its effect on ozone  
706 production during the HaChi summer campaign, *Atmos. Chem. Phys.*, 11, 4657-4667,  
707 10.5194/acp-11-4657-2011, 2011.

708 Safai, P. D., Kewat, S., Pandithurai, G., Praveen, P. S., Ali, K., Tiwari, S., Rao, P. S. P., Budhawant,  
709 K. B., Saha, S. K., and Devara, P. C. S.: Aerosol characteristics during winter fog at Agra, North  
710 India, *J. Atmos. Chem.*, 61, 101-118, 10.1007/s10874-009-9127-4, 2008.

711 [Shen, C., Zhao, C., Ma, N., Tao, J., Zhao, G., Yu, Y., and Kuang, Y.: Method to Estimate Water](#)  
712 [Vapor Supersaturation in the Ambient Activation Process Using Aerosol and Droplet](#)  
713 [Measurement Data, \*Journal of Geophysical Research: Atmospheres\*, 123, 10606-10619,](#)  
714 [doi:10.1029/2018JD028315, 2018.](#)

715 Song, S., Gao, M., Xu, W., Shao, J., Shi, G., Wang, S., Wang, Y., Sun, Y., and McElroy, M. B.:  
716 Fine-particle pH for Beijing winter haze as inferred from different thermodynamic equilibrium  
717 models, *Atmos. Chem. Phys.*, 18, 7423-7438, 10.5194/acp-18-7423-2018, 2018.

718 [Stutz, J., Alicke, B., and Neftel, A.: Nitrous acid formation in the urban atmosphere: Gradient](#)  
719 [measurements of NO<sub>2</sub> and HONO over grass in Milan, Italy, \*Journal of Geophysical Research:\*](#)  
720 [Atmospheres, 107, LOP 5-1-LOP 5-15, doi:10.1029/2001JD000390, 2002.](#)

721 Su, H., Cheng, Y., Oswald, R., Behrendt, T., Trebs, I., Meixner, F. X., Andreae, M. O., Cheng, P.,  
722 Zhang, Y., and Pöschl, U.: Soil Nitrite as a Source of Atmospheric HONO and OH Radicals,  
723 *Science*, 333, 1616-1618, 10.1126/science.1207687, 2011.

724 [Teng, X., Hu, Q., Zhang, L., Qi, J., Shi, J., Xie, H., Gao, H., and Yao, X.: Identification of Major](#)  
725 [Sources of Atmospheric NH<sub>3</sub> in an Urban Environment in Northern China During Wintertime,  
726 \[Environmental Science & Technology, 51, 6839-6848, 10.1021/acs.est.7b00328, 2017.\]\(#\)](#)

带格式的: 两端对齐

带格式的: 两端对齐

带格式的: 两端对齐



727 [Vogel, B., Vogel, H., Kleffmann, J., and Kurtenbach, R.: Measured and simulated vertical profiles](#)  
728 [of nitrous acid—Part II. Model simulations and indications for a photolytic source, Atmospheric](#)  
729 [Environment, 37, 2957-2966, \[https://doi.org/10.1016/S1352-2310\\(03\\)00243-7\]\(https://doi.org/10.1016/S1352-2310\(03\)00243-7\), 2003.](#)

730 Wang, G., Zhang, R., Gomez, M. E., Yang, L., Levy Zamora, M., Hu, M., Lin, Y., Peng, J., Guo,  
731 S., Meng, J., Li, J., Cheng, C., Hu, T., Ren, Y., Wang, Y., Gao, J., Cao, J., An, Z., Zhou, W., Li,  
732 G., Wang, J., Tian, P., Marrero-Ortiz, W., Secrest, J., Du, Z., Zheng, J., Shang, D., Zeng, L., Shao,  
733 M., Wang, W., Huang, Y., Wang, Y., Zhu, Y., Li, Y., Hu, J., Pan, B., Cai, L., Cheng, Y., Ji, Y.,  
734 Zhang, F., Rosenfeld, D., Liss, P. S., Duce, R. A., Kolb, C. E., and Molina, M. J.: Persistent sulfate  
735 formation from London Fog to Chinese haze, *Proceedings of the National Academy of Sciences*,  
736 [113, 13630, 2016a](#)[10.1073/pnas.1616540113](#), 2016.

737 Wang, G., Zhang, R., Gomez, M. E., Yang, L., Levy Zamora, M., Hu, M., Lin, Y., Peng, J., Guo,  
738 S., Meng, J., Li, J., Cheng, C., Hu, T., Ren, Y., Wang, Y., Gao, J., Cao, J., An, Z., Zhou, W., Li,  
739 G., Wang, J., Tian, P., Marrero-Ortiz, W., Secrest, J., Du, Z., Zheng, J., Shang, D., Zeng, L.,  
740 Shao, M., Wang, W., Huang, Y., Wang, Y., Zhu, Y., Li, Y., Hu, J., Pan, B., Cai, L., Cheng, Y.,  
741 Ji, Y., Zhang, F., Rosenfeld, D., Liss, P. S., Duce, R. A., Kolb, C. E., and Molina, M. J.:  
742 [Persistent sulfate formation from London Fog to Chinese haze, \*Proc Natl Acad Sci U S A\*,  
743 \[10.1073/pnas.1616540113\]\(#\), 2016b.](#)

744 Whalley, L. K., Stone, D., George, I. J., Mertes, S., van Pinxteren, D., Tilgner, A., Herrmann, H.,  
745 Evans, M. J., and Heard, D. E.: [The influence of clouds on radical concentrations: observations](#)  
746 [and modelling studies of HO<sub>x</sub> during the Hill Cap Cloud Thuringia \(HCCT\)](#)  
747 [campaign in 2010, \*Atmos. Chem. Phys.\*, 15, 3289-3301, 10.5194/acp-15-3289-2015](#), 2015.

748 Wu, Z., Wang, Y., Tan, T., Zhu, Y., Li, M., Shang, D., Wang, H., Lu, K., Guo, S., Zeng, L., and  
749 Zhang, Y.: Aerosol Liquid Water Driven by Anthropogenic Inorganic Salts: Implying Its Key Role  
750 in Haze Formation over the North China Plain, *Environmental Science & Technology Letters*,  
751 [10.1021/acs.estlett.8b00021](#), 2018.

752 Xing, J., Ding, D., Wang, S., Zhao, B., Jang, C., Wu, W., Zhang, F., Zhu, Y., and Hao, J.:  
753 Quantification of the enhanced effectiveness of NO<sub>x</sub> control from simultaneous reductions of  
754 VOC and NH<sub>3</sub> for reducing air pollution in the Beijing–Tianjin–Hebei region, China, *Atmos.*  
755 *Chem. Phys.*, 18, 7799-7814, 10.5194/acp-18-7799-2018, 2018.

756 Xu, W. Y., Zhao, C. S., Ran, L., Lin, W. L., Yan, P., and Xu, X. B.: SO<sub>2</sub> noontime-peak  
757 phenomenon in the North China Plain, *Atmospheric Chemistry and Physics*, 14, 7757-7768,  
758 [10.5194/acp-14-7757-2014](#), 2014.

759 [Xue, L. K., Wang, T., Gao, J., Ding, A. J., Zhou, X. H., Blake, D. R., Wang, X. F., Saunders, S.](#)  
760 [M., Fan, S. J., Zuo, H. C., Zhang, Q. Z., and Wang, W. X.: Ground-level ozone in four Chinese](#)  
761 [cities: precursors, regional transport and heterogeneous processes, \*Atmos. Chem. Phys.\*, 14,  
762 \[13175-13188, 10.5194/acp-14-13175-2014\]\(#\), 2014.](#)

763 Yabushita, A., Enami, S., Sakamoto, Y., Kawasaki, M., Hoffmann, M. R., and Colussi, A. J.:  
764 Anion-Catalyzed Dissolution of NO<sub>2</sub> on Aqueous Microdroplets, *The Journal of Physical*  
765 *Chemistry A*, 113, 4844-4848, 10.1021/jp900685f, 2009.

766 [Ye, C., Liu, P., Ma, Z., Xue, C., Zhang, C., Zhang, Y., Liu, J., Liu, C., Sun, X., and Mu, Y.: High](#)  
767 [H<sub>2</sub>O<sub>2</sub> Concentrations Observed during Haze Periods during the Winter in Beijing: Importance of](#)  
768 [H<sub>2</sub>O<sub>2</sub> Oxidation in Sulfate Formation, \*Environmental Science & Technology Letters\*,](#)  
769 [10.1021/acs.estlett.8b00579](#), 2018.

770 Yin, Z., Ye, X., Jiang, S., Tao, Y., Shi, Y., Yang, X., and Chen, J.: Size-resolved effective density  
771 of urban aerosols in Shanghai, *Atmospheric Environment*, 100, 133-140,  
772 [http://dx.doi.org/10.1016/j.atmosenv.2014.10.055](#), 2015.

带格式的: 两端对齐

带格式的: 两端对齐

带格式的: 两端对齐

带格式的: 两端对齐



Young, L.-H., Li, C.-H., Lin, M.-Y., Hwang, B.-F., Hsu, H.-T., Chen, Y.-C., Jung, C.-R., Chen, K.-C., Cheng, D.-H., Wang, V.-S., Chiang, H.-C., and Tsai, P.-J.: Field performance of a semi-continuous monitor for ambient PM<sub>2.5</sub> water-soluble inorganic ions and gases at a suburban site, *Atmospheric Environment*, 144, 376-388, <https://doi.org/10.1016/j.atmosenv.2016.08.062>, <https://doi.org/10.1016/j.atmosenv.2016.08.062>, 2016.

Zheng, G. J., Duan, F. K., Su, H., Ma, Y. L., Cheng, Y., Zheng, B., Zhang, Q., Huang, T., Kimoto, T., Chang, D., Pöschl, U., Cheng, Y. F., and He, K. B.: Exploring the severe winter haze in Beijing: the impact of synoptic weather, regional transport and heterogeneous reactions, *Atmos. Chem. Phys.*, 15, 2969-2983, 10.5194/acp-15-2969-2015, 2015.

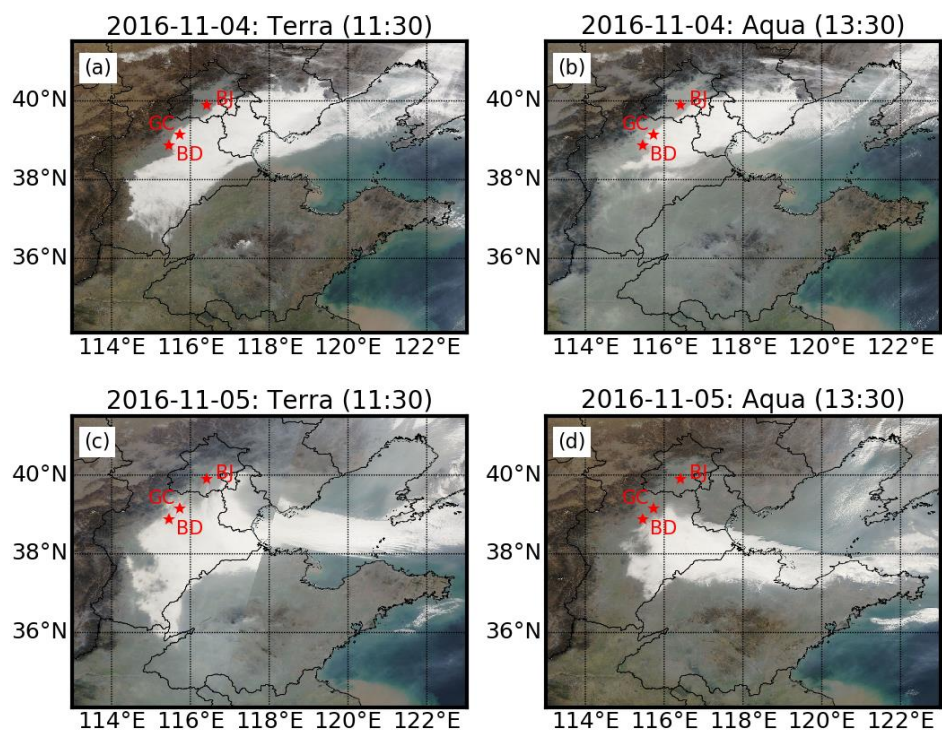
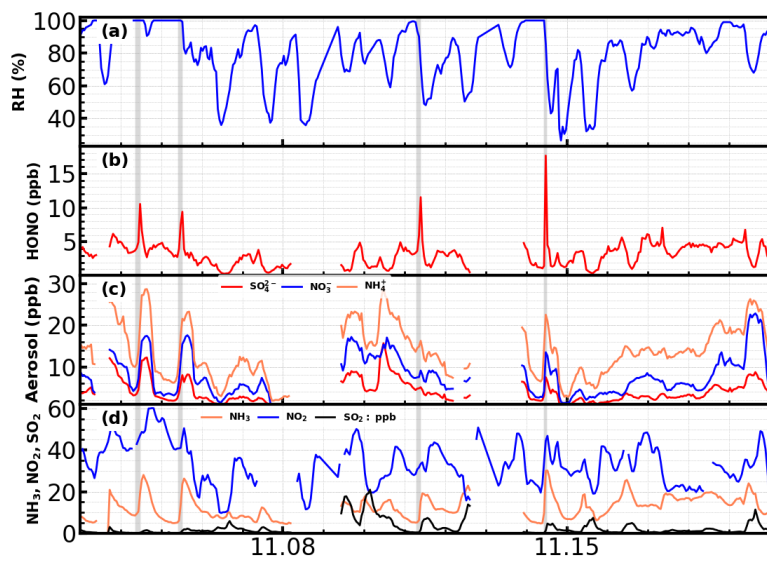
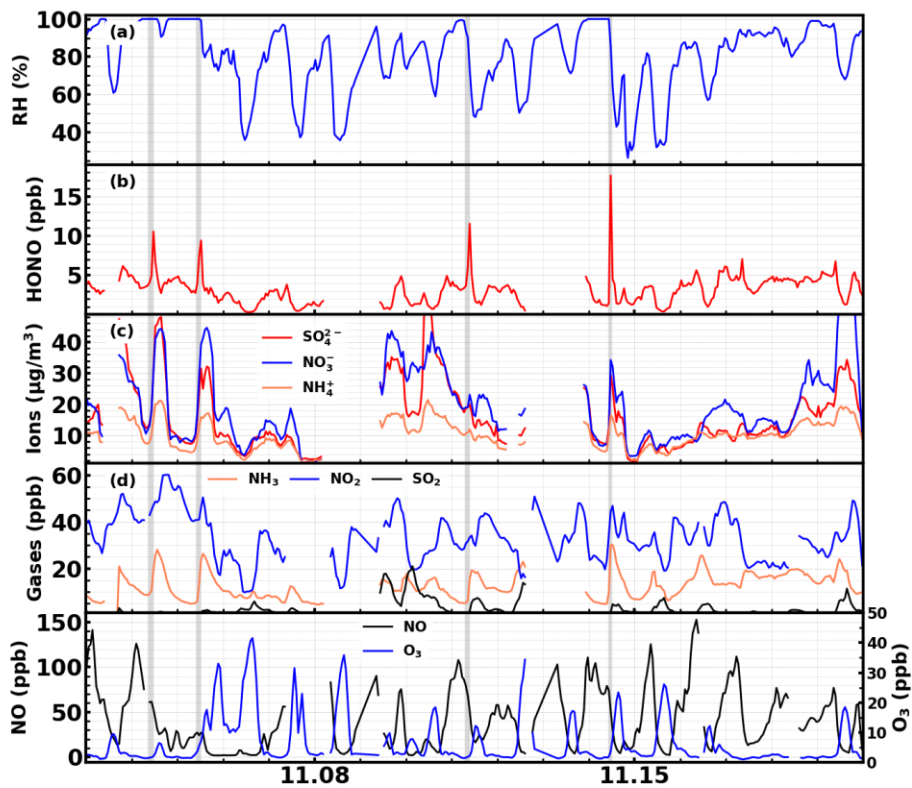


**Figure 1.** MODIS Terra (a,c) and Aqua (b,d) satellite images in [2016-11-04](#)<sup>th</sup> Nov. (a,b) and [5<sup>th</sup> Nov.](#) 2016-~~11-05~~ (c,d), star markers are locations of Gucheng (GC: the observation site), Baoding (BD) and Beijing (BJ).

带格式的: 1 级

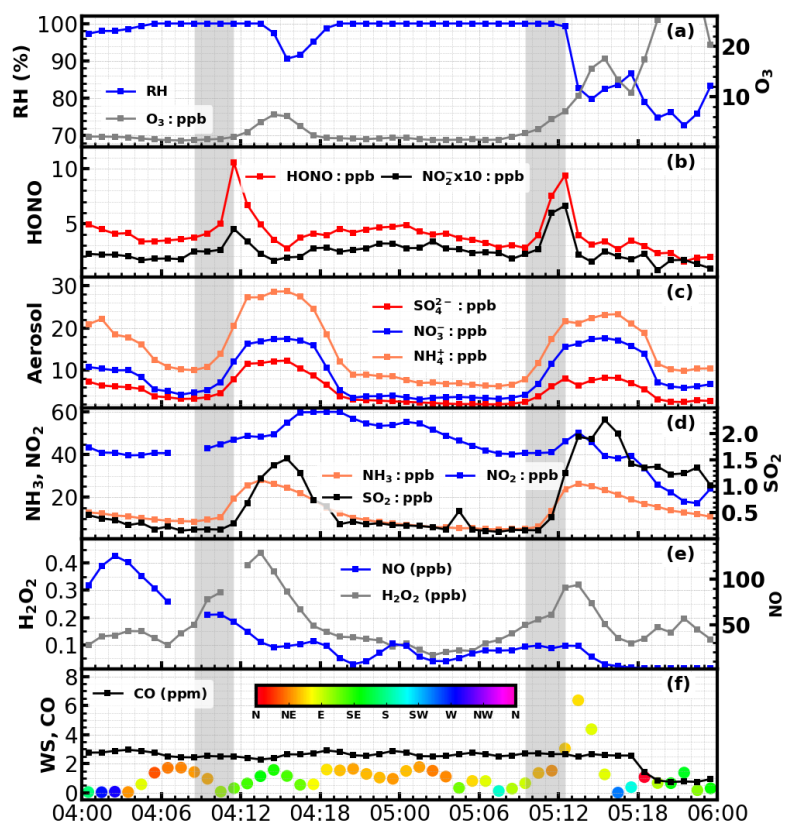


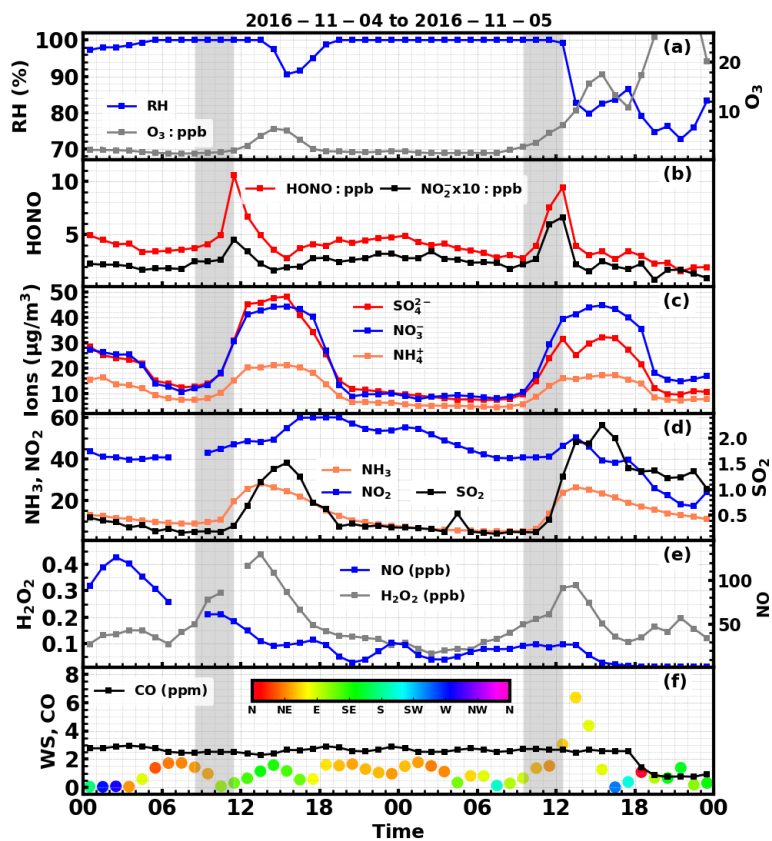
799



**Figure 2.** Time series of ambient a) RH; b) HONO; c) sulfate, nitrate, ammonium; d) NH<sub>3</sub>, NO<sub>3</sub><sup>-</sup> and SO<sub>2</sub> during the observation period.

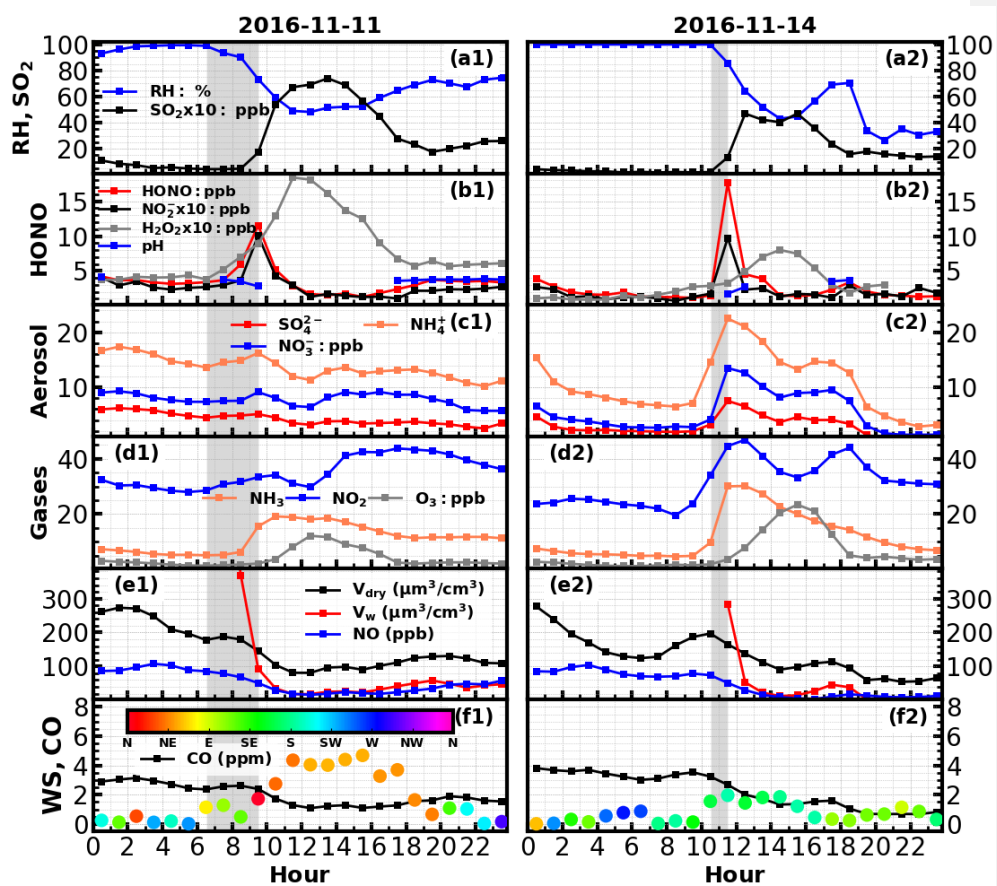
带格式的: 1 级





**Figure 3.** Time series of ambient **a)** RH, O<sub>3</sub>, **b)** HONO, NO<sub>2</sub>, **c)** SO<sub>4</sub><sup>2-</sup>, NO<sub>3</sub><sup>-</sup>, NH<sub>4</sub><sup>+</sup>, **d)** NH<sub>3</sub>, NO<sub>2</sub>, SO<sub>2</sub>, **e)** NO, H<sub>2</sub>O<sub>2</sub>, **f)** CO, wind speed and wind direction (colors of scatter points) from 11-04<sup>th</sup> to 11-05<sup>th</sup> Nov. 2016. Gray shaded areas represent periods of rapid increase of HONO.

带格式的: 1 级





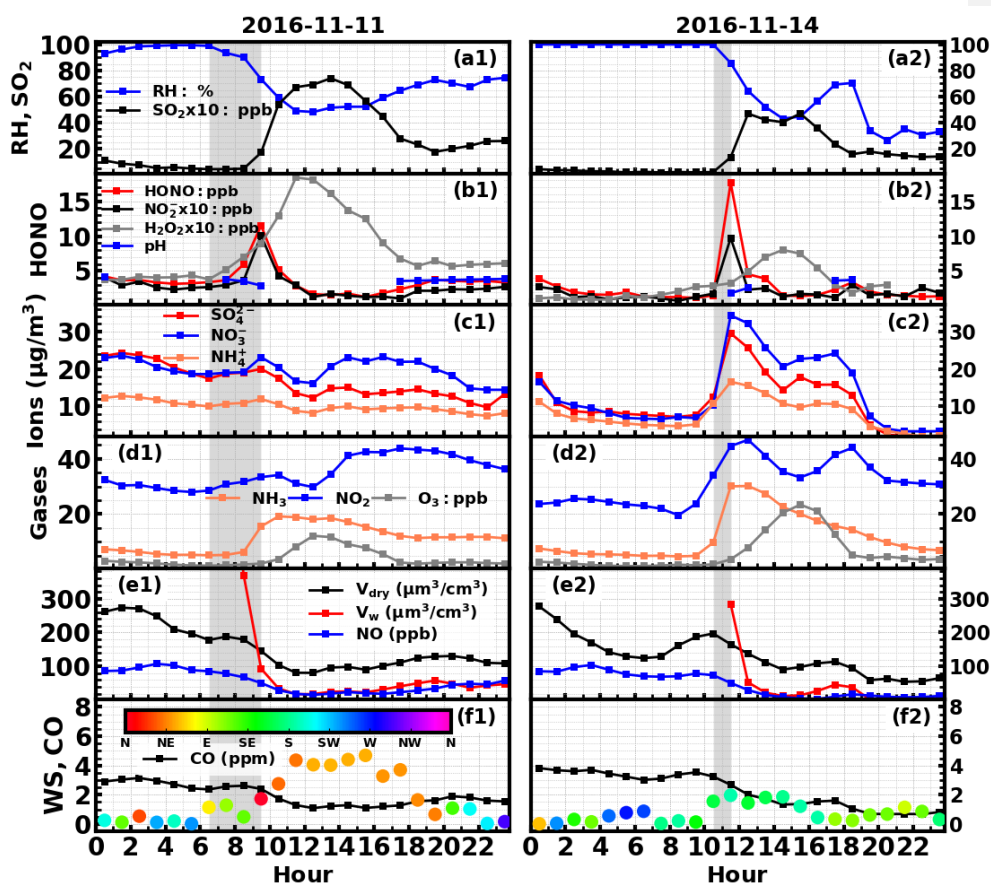


**Figure 4.** Time series of ambient **a)** RH, SO<sub>2</sub>, **b)** HONO, NO<sub>2</sub><sup>-</sup>, H<sub>2</sub>O<sub>2</sub>, aerosol pH, **c)** SO<sub>4</sub><sup>2-</sup>, NO<sub>3</sub><sup>-</sup>, NH<sub>4</sub><sup>+</sup>, **d)** NH<sub>3</sub>, NO<sub>2</sub>, O<sub>3</sub>, **e)** NO, volume concentrations of PM<sub>2.5</sub> in dry state (V<sub>dry</sub>), volume concentrations of liquid water (V<sub>w</sub>), **f)** CO, wind speed and wind direction during **1)** 11<sup>th</sup> Nov. 2016 and **2)** 14<sup>th</sup> Nov. 2016. Gray shaded areas represents periods of rapid increase of HONO.

带格式的: 1 级



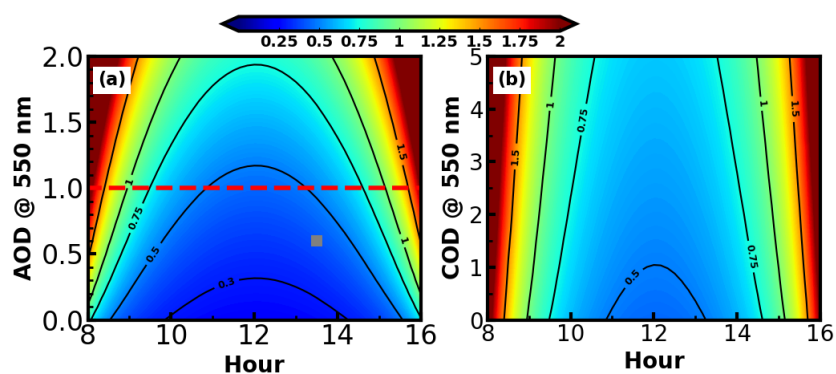


**Figure 5.** (a) Diurnal variations of lifetime of HONO under different aerosol optical depth (AOD) conditions. Gray solid marker represents the AOD position from MODIS Aqua in 2016-11-14 (about 13:30); (b) Diurnal variations of lifetime of HONO under different cloud optical depth (COD) conditions, with an AOD of 1.

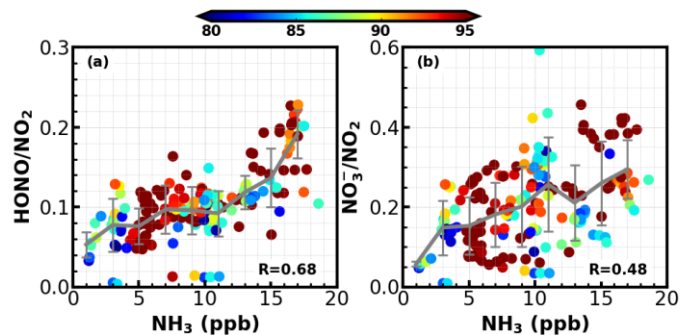


Figure 6.

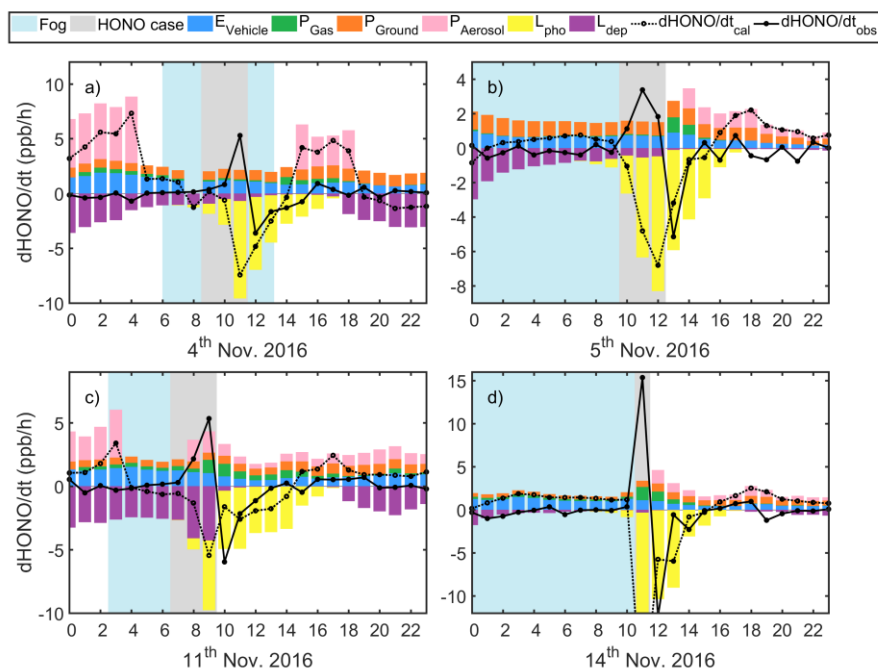
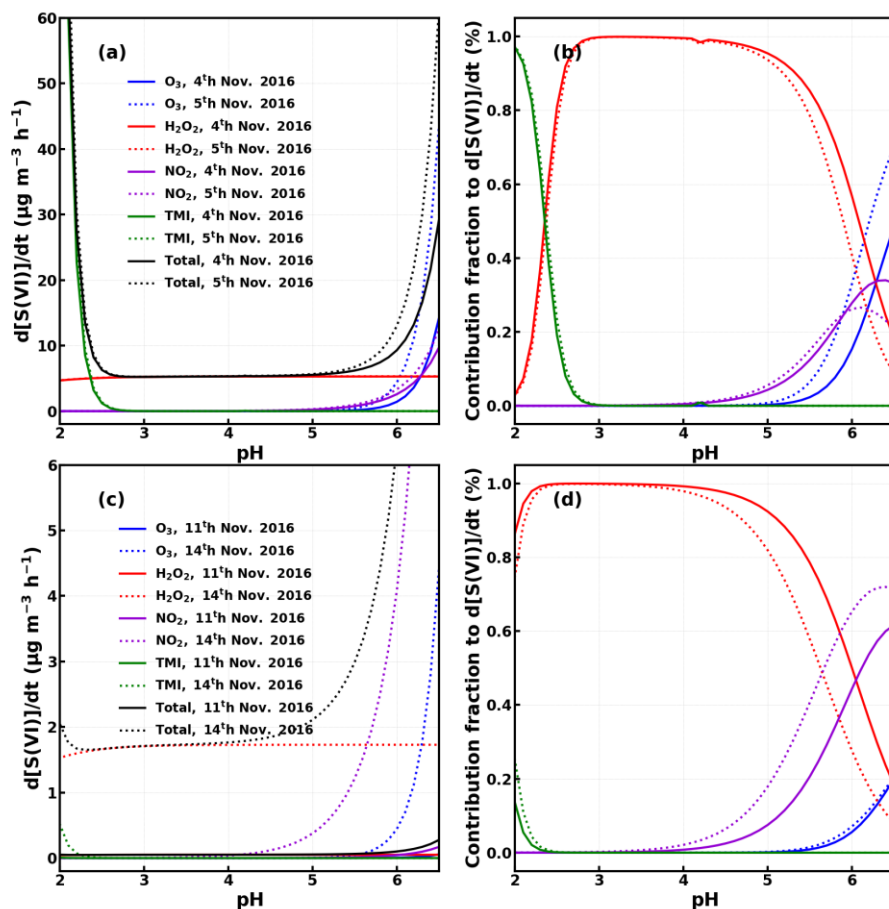
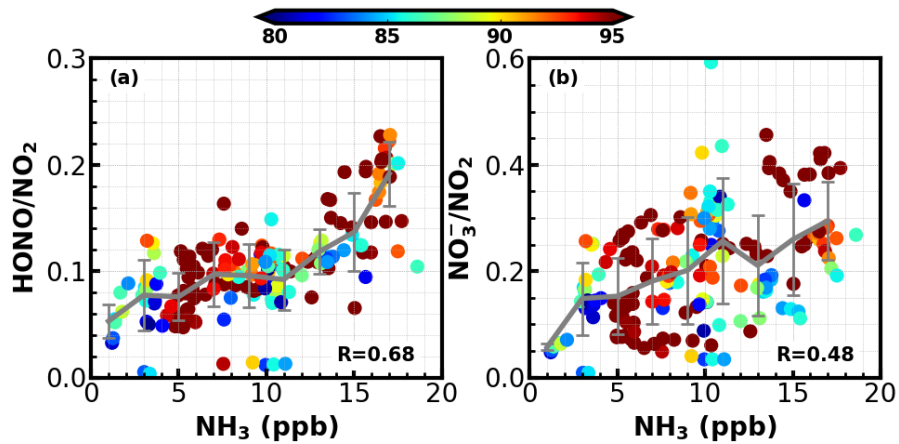


Figure 5. Estimated HONO emission from vehicles (blue), gas phase production (green), production on ground (orange) and aerosol surface (pink), loss through photolysis (yellow) and dry deposition (purple), as well as the calculated (dotted black) and actually observed (solid black)  $d[HONO]/dt$  on a) 4<sup>th</sup>, b) 5<sup>th</sup>, c) 11<sup>th</sup> and d) 14<sup>th</sup> Nov. 2016



**Figure 6.** Calculated average sulfate production (a,c) and contribution fraction b,d) from  $\text{SO}_2$  oxidation by  $\text{H}_2\text{O}_2$ ,  $\text{NO}_2$ ,  $\text{O}_3$ , TMI under different pH values using methods described in (Cheng et al., 2016) for the case episodes on 4<sup>th</sup>, 5<sup>th</sup>, 11<sup>th</sup> and 14<sup>th</sup> Nov. 2016.



**Figure 7.** The relationship between  $\text{NH}_3$  concentration and **a)**  $\text{HONO}/\text{NO}_2$  ratio; **b)** nitrate/nitrogen dioxide ratio ( $\text{NO}_3^-/\text{NO}_2$ ); Colors of scatter points represent ambient RHs and the color bar is shown on the top.

带格式的: 1 级

设置了格式: 字体: 小四

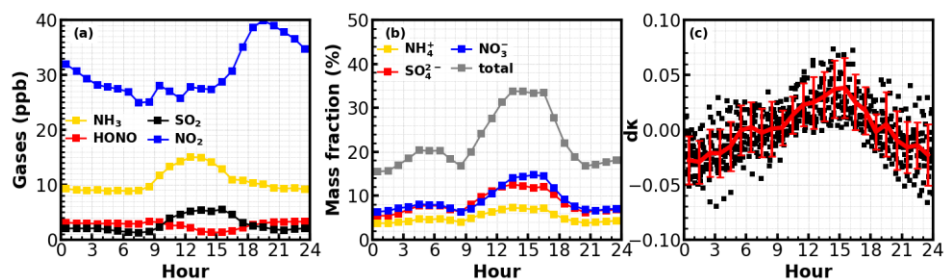


**Figure 78.** (a) Average diurnal variations of Gases; (b) Average diurnal variations mass fractions of nitrate, sulfate and ammonium; (c) Diurnal variations of aerosol hygroscopicity,  $dk$  is the anomaly to the daily mean  $\kappa$ .

带格式的: 两端对齐, 1 级